LHC Signatures of a Minimal Supersymmetric Hidden Valley

Yuk Fung Chan[(a,c)], Matthew Low[(b,c)],
David E. Morrissey[(c)], and Andrew P. Spray[(c)]

(a) Program in Applied and Computational Mathematics, Princeton University, Princeton, NJ 08544, USA
(b) Enrico Fermi Institute, University of Chicago, 5640 South Ellis Avenue, Chicago, IL 60637, USA
(c) TRIUMF, 4004 Wesbrook Mall, Vancouver, BC V6T 2A3, Canada

email: dmorri@triumf.ca, aps37@triumf.ca

June 28, 2012

Abstract

We investigate the LHC signals of a minimal supersymmetric hidden valley. Our theory consists of the supersymmetric Standard Model along with a light hidden $U(1)_x$ gauge multiplet and a pair of hidden chiral superfields that spontaneously break the new Abelian gauge symmetry near a GeV. The visible and hidden sectors interact exclusively through supersymmetric gauge kinetic mixing. We perform a thorough examination of the hidden decay cascades initiated by the lightest Standard Model superpartner and we study the range of LHC signals they can produce. In particular, we find parameter regions that give rise to missing energy, single and multiple lepton jets, and displaced vertices. Given the simplicity of the underlying theory and the broad range of collider signals it can produce, we propose that this model is a useful benchmark for LHC studies of (supersymmetric) hidden valleys.

1 Introduction

The Large Hadron Collider (LHC) is rapidly collecting data from high energy proton (pp) collisions with a center of mass energy of $\sqrt{s} = 7$ TeV. Precision measurements of collision events by the ATLAS and CMS detectors may lead to the discovery of new physical phenomena beyond those predicted by the Standard Model (SM) of particle physics. In order to maximize the experimental reach for such new discoveries, it is necessary to search broadly within the data. For this, it is helpful to have a diverse set of theoretical benchmarks to compare against observations [1].

Hidden valley (HV) models are an interesting and well-motivated class of new physics that could be discovered at the LHC. However, compared to many other theories of exotic particle physics phenomena, their signatures at the LHC have been studied in much less detail. HV models can also be challenging to find at the LHC, leading to events that are not picked up by the more standard searches for new physics [2–4]. For these reasons, in the present work we present and investigate a minimal supersymmetric HV theory that can serve as a benchmark for future collider searches.

A generic HV theory consists of three components [2]: a visible sector of particles containing the SM, a hidden sector consisting of particles that couple feebly to the SM, and some mediator states that couple efficiently to both the visible and the hidden sectors. Furthermore, the hidden sector is typically assumed to have a characteristic mass well below the electroweak scale while the mediators have TeV-scale masses.[1] The presence of mediators coupling to the SM allows for the abundant production of hidden particles at high-energy colliders. When a mediator is created, it can decay to light HV states and populate the valley. In turn, the light hidden particles can be stable, or more interestingly they might be able to decay back to the SM. This broad paradigm of new physics scenarios can give rise to an equally broad range of collider signals, including missing energy ($\not{E}_T$), displaced vertices, and high particle multiplicities.

Low-scale supersymmetry with R-parity provides a particularly promising and effective mediator to a hidden valley. Once produced, SM superpartners will decay in a cascade down to the lightest SM superpartner (LSMP). However, if there are lighter superpartners among the hidden states, the

[1] All of these mass scales can be natural in the context of supersymmetry [5–7] or strong coupling/warping [2, 8].

LSMP will be unstable against decaying into one of them. The decay cascade would then continue within the hidden valley until the true lightest superpartner (LSP), now derived from the hidden sector, is produced. Along the way, several hidden particles decaying back to the SM could also be generated. The net collider signature of such an event would therefore consist of the direct products of the supersymmetric SM cascade, together with missing energy from the LSP, and the products of the HV decays.

In this paper we investigate the collider signals of a simple and minimal supersymmetric hidden valley. The theory consists of the minimal supersymmetric standard model (MSSM) together with a much lighter hidden sector consisting of a supersymmetric $U(1)_x$ gauge multiplet and a pair of chiral multiplets H and H' that spontaneously break the new gauge symmetry at an energy scale well below the electroweak. The MSSM and hidden sectors are assumed to couple exclusively through a gauge kinetic mixing interaction [9].

Despite its minimality, this theory gives rise to a rich variety of collider signatures. As such, it provides a simple but useful benchmark model to guide LHC searches for hidden valleys. Even so, we emphasize that this model does not come close to covering the full range of possible collider signals that can emerge from the HV paradigm. Related studies of supersymmetric hidden valleys have appeared in Refs. [6,10–14]. Relative to these previous works, we focus on a single specific hidden sector theory for which we perform a detailed investigation of the possible hidden decay cascades, we take into account the entire structure of the hidden sector, and we attempt to characterize the full range of collider signals that it can produce.

The outline of this paper is as follows. In Sec. 2 we present our benchmark hidden valley in detail, while in Sec. 3 we investigate some its general features that are relevant for LHC phenomenology. We perform a scan over the parameters characterizing the HV in Sec. 4 to classify the range of hidden cascade topologies. In Sec. 5 we study the LHC signals of five specific sample parameter points. Finally, Sec. 6 is reserved for our conclusions. Some additional technical details are contained in Appendices A, B and C.

2 Model

Our model is the minimal extension of the MSSM by a new spontaneously broken $U(1)_x$ gauge group. In this sense, it is also a minimal supersymmetric hidden valley. We review the pertinent features of the model here; for more details see Ref. [7].

2.1 Fields and Interactions

The hidden sector consists of the exotic $U(1)_x$ vector superfield X and two chiral superfields H and H' responsible for breaking the hidden gauge symmetry. Both are neutral under the SM gauge symmetries but have $U(1)_x$ charges ± 1; while all MSSM superfields are neutral under $U(1)_x$. The superpotential is extended by a hidden mass term

$$W = W_{MSSM} - \mu' \, H \, H'. \tag{1}$$

The Kähler potential is taken to be canonical, while the gauge kinetic terms include mixing between X and the hypercharge superfield B:

$$\begin{aligned} \mathcal{L} &\supset \frac{1}{4} \int d^2\theta \left(X^\alpha X_\alpha + 2\epsilon \, B^\alpha X_\alpha + B^\alpha B_\alpha \right) + h.c. \\ &\supset \epsilon \left(-\frac{1}{2} B_{\mu\nu} X^{\mu\nu} + \frac{i}{2} \, \tilde{B}^\dagger \bar{\sigma} \cdot \partial \tilde{X} + \frac{i}{2} \tilde{X}^\dagger \bar{\sigma} \cdot \partial \tilde{B} + D_Y D_X \right). \end{aligned} \tag{2}$$

This term can be naturally induced by integrating out heavy fields charged under both hypercharge and $U(1)_x$, in which case values of $\epsilon \sim 10^{-4} - 10^{-2}$ are typical. Note that in terms of component fields, we have kinetic mixing of the gauge fields and the gauginos, as well as D-term mixing that will contribute to the scalar potential.

We will be largely agnostic about the specific method of SUSY breaking, assuming only that the hidden sector soft masses are real and less than or on the order of a GeV. An explicit mechanism that realizes this spectrum of soft masses in a natural way is gauge mediation by gauge messengers charged under the MSSM but neutral under the hidden $U(1)_x$. This leads to hidden sector soft parameters on the order $\epsilon \, m_{MSSM} \lesssim$ GeV. To avoid a cosmologically troublesome light fermion in this scenario [7], additional GeV-scale supergravity contributions are needed, and these also provide a natural origin for the μ' term through the Giudice-Masiero mechanism [15]. As such,

in this mechanism the soft terms of the hidden sector are not calculable without an underlying theory of supergravity, and we treat them as free parameters. The relevant supersymmetry-breaking operators are[2]

$$-\mathcal{L}_{\text{hid, soft}} = m_H^2 |H|^2 + m_{H'}^2 |H'|^2 + \left(-b' H H' + \frac{1}{2} M_x \tilde{X} \tilde{X} + h.c. \right), \quad (3)$$

where we may take b' and M_x positive without loss of generality.

The cost of making b' and M_x both real and positive is that there can remain a physical CP-violating phase in μ'. As mentioned above, we will assume that μ' is real (but not necessarily positive) as well. This is done largely for convenience, since a full exploration of the effects of hidden-sector CP violation lies beyond the scope of this paper. However, will comment on the qualitative implications on the mass spectrum and mixing matrices in Sec. 2.2, and on the decay modes in Sec. 3.

Electroweak symmetry breaking in the MSSM introduces additional contributions to the hidden sector scalar potential. The MSSM Higgs vacuum expectation values (VEVs) induce a non-vanishing hypercharge D-term

$$\langle D_Y \rangle \equiv \xi_Y = -\frac{g_Y}{2} \cos 2\beta \, v^2. \quad (4)$$

The $D_Y D_X$ term in (2) then leads to an effective Fayet-Iliopoulos term [16] for the hidden sector. This term can be absorbed by shifting the hidden Higgs soft masses according to

$$m_H^2 \to \tilde{m}_H^2 = m_H^2 - \epsilon \, g_x \xi_Y \,, \quad m_{H'}^2 \to \tilde{m}_{H'}^2 = m_{H'}^2 + \epsilon \, g_x \xi_Y \,. \quad (5)$$

Note that this contribution would break supersymmetry in the hidden sector even if it were isolated from all other sources of breaking.

2.2 Hidden Sector Masses and Mixings

We demand that the $U(1)_x$ gauge symmetry is spontaneously broken by a non-zero VEV of H or H'. Since the hidden scalar potential is structurally identical to that of the neutral MSSM Higgses (at tree-level), both hidden scalar expectation values can be taken positive,

$$\langle H \rangle = \eta \, \sin\zeta \,, \qquad \langle H' \rangle = \eta \, \cos\zeta \,, \quad (6)$$

[2] We neglect a possible mass term mixing $\tilde{X}$ and $\tilde{B}$. No such term is generated from gauge mediation to the MSSM alone [7], and the residual gravity-mediated contribution is on the order of $\epsilon \, M_x \ll M_x$.

with $\zeta \in [0, \pi/2]$. In terms of the underlying Lagrangian parameters, we have (neglecting $\mathcal{O}(\epsilon^2)$ corrections)

$$\sin 2\zeta = \frac{2b'}{2|\mu'|^2 + \tilde{m}_H^2 + \tilde{m}_{H'}^2}\,, \tag{7}$$

$$\eta^2 = -\frac{|\mu'|^2}{g_x^2} + \frac{-\tilde{m}_H^2 \tan^2\zeta + \tilde{m}_{H'}^2}{g_x^2(\tan^2\zeta - 1)}\,. \tag{8}$$

As a result of the symmetry breaking, the hidden gauge boson acquires a mass of

$$m_x = \sqrt{2}\, g_x \eta\,. \tag{9}$$

These results apply for vanishing kinetic mixing. We will show below that the modifications to these expressions from the mixing are negligibly small.

After $U(1)_x$ breaking, there are seven physical states in the hidden sector: the gauge boson X_μ, two real scalars $h^x_{1,2}$ and a pseudoscalar A^x, and three Majorana fermions χ^x_j. The hidden sector introduces seven new parameters compared to the MSSM, which we take to be ϵ, g_x, μ', M_x, m_x, $\tan\zeta$ and the pseudoscalar mass m_{A^x}.

We turn next to the gauge kinetic mixing. The neutral gauge boson quadratic terms are

$$\begin{aligned}\mathcal{L} \supset -\frac{1}{4}X^{\mu\nu}X_{\mu\nu} - \frac{1}{4}A^{\mu\nu}A_{\mu\nu} - \frac{1}{4}Z^{\mu\nu}Z_{\mu\nu} - \frac{\epsilon}{2}X^{\mu\nu}\big(c_W A_{\mu\nu} - s_W Z_{\mu\nu}\big) \\ + \frac{1}{2}m_x^2 X^\mu X_\mu + \frac{1}{2}m_Z^2 Z^\mu Z_\mu\,,\end{aligned} \tag{10}$$

where $s_W\,(c_W) = \sin\theta_W\,(\cos\theta_W)$. To linear order in ϵ, we can remove the kinetic mixing by the transformations[3]

$$\begin{aligned} X_\mu &\to X_\mu + \epsilon\, s_W Z_\mu\,, \\ Z_\mu &\to Z_\mu\,, \\ A_\mu &\to A_\mu - \epsilon\, c_W X_\mu\,. \end{aligned} \tag{11}$$

This rotation introduces a mass mixing between X_μ and Z_μ. However, the mixing is suppressed by both ϵ and m_x^2/m_Z^2, and so can be safely ignored. The rotation also induces a coupling of the X vector boson to the MSSM with effective charge $-\epsilon\, c_W (e/g_X)$, and a coupling of the Z boson to all the hidden scalars and fermions with strength proportional to $\epsilon\, s_W$.

[3]It is straightforward to generalise these expressions to all orders in ϵ.

The Bino-Xino kinetic mixing can be most conveniently removed by the field rotation (again dropping terms $\mathcal{O}(\epsilon^2)$)

$$\begin{aligned} \tilde{X} &\to \tilde{X} - \epsilon \tilde{B}\,, \\ \tilde{B} &\to \tilde{B}\,. \end{aligned} \tag{12}$$

This introduces a mass mixing between the hidden and visible neutralinos. The resultant mixing angle is less than or on the order of $\epsilon m_{\chi_1^x}/m_{\chi_1^0}$. Since this angle is expected to be very small, we diagonalize the hidden and visible neutralino mass matrices independently, and treat the mixing in the mass insertion approximation in the few cases where it is relevant.

The four visible sector neutralinos simply mix as in the MSSM. The mass matrix for the three hidden sector fermions is given in the basis $\tilde{\psi}^x \equiv (\tilde{H}, \tilde{H}', \tilde{X})^t$ by

$$\mathcal{M}_X = \begin{pmatrix} 0 & -\mu' & m_x s_\zeta \\ -\mu' & 0 & -m_x c_\zeta \\ m_x s_\zeta & -m_x c_\zeta & M_x \end{pmatrix}. \tag{13}$$

We relate the gauge and mass eigenstates by an analogue of the SLHA convention for the MSSM [17]. Explicitly,

$$\psi_j^x = P_{ij}^* \chi_i^x\,, \tag{14}$$

where P is a unitary matrix. As all hidden soft parameters are assumed to be real, we take P to have strictly real entries at the cost of allowing some of the χ_j^x mass eigenvalues to be negative, which we sort by $\left|m_{\chi_1^x}\right| \le \left|m_{\chi_2^x}\right| \le \left|m_{\chi_3^x}\right|$.

Among the scalars, there is no kinetic mixing between between the visible and hidden sectors. However, there is mass mixing among the CP-even states induced by the D-term mixing. Since the resultant mixing angles are very small, on the order of $\epsilon\, m_x/m_Z \ll 1$, it is a good approximation to diagonalize the hidden and visible scalar sector mass matrices independently and treat the mixing as a mass insertion interaction when it is needed.

In the hidden sector this produces two CP-even states h_1^x and h_2^x and a CP-odd A^x. The hidden pseudoscalar A^x mass is

$$m_{A^x}^2 = \frac{2b'}{\sin 2\zeta} = 2|\mu'|^2 + \tilde{m}_H^2 + \tilde{m}_{H'}^2\,. \tag{15}$$

For the two CP-even states, h_1^x and h_2^x, the mass matrix is given by

$$\mathcal{M}_{h^x}^2 = \begin{pmatrix} m_x^2 s_\zeta^2 + m_{A^x}^2 c_\zeta^2 & -(m_x^2 + m_{A^x}^2) s_\zeta c_\zeta \\ -(m_x^2 + m_{A^x}^2) s_\zeta c_\zeta & m_x^2 c_\zeta^2 + m_{A^x}^2 s_\zeta^2 \end{pmatrix}. \tag{16}$$

Due to the structural similarity to the MSSM, it follows that the lighter mass eigenstate h_1^x has mass bounded from above by both $m_x\,|\cos 2\zeta|$ and $m_{A^x}\,|\cos 2\zeta|$. The heavier CP-even scalar is in turn bounded from below, as $m_{h_1^x}^2 + m_{h_2^x}^2 = m_x^2 + m_{A^x}^2$. The expansion of H, H' in terms of the mass basis is

$$\begin{aligned} H &= \eta\,\sin\zeta + \frac{1}{\sqrt{2}}\big(R_{1a}h_a^x + i\,\cos\zeta\,A^x\big)\,, \\ H' &= \eta\,\cos\zeta + \frac{1}{\sqrt{2}}\big(R_{2a}h_a^x + i\,\sin\zeta\,A^x\big)\,, \end{aligned} \tag{17}$$

where R is the orthogonal matrix that diagonalizes the real symmetric matrix in Eq. (16).

Let us comment upon the modifications to these results when we allow the hidden sector parameters to be complex. The fact that we can rotate away any phase associated with b' means that at tree level all our results for the scalars are unchanged. In particular, the hidden Higgses can not spontaneously break CP. We would expect loop corrections to mix A^x with $h_{1,2}^x$, but this should not significantly alter the spectrum or h_1^x–h_2^x mixing. In the fermion sector, we can no longer choose the mixing matrix P to be real, but there are no qualitatively new effects.

For completeness, we collect a list of the most important interaction terms within the hidden sector in Appendix A. These interactions are expressed in terms of both gauge and mass eigenstates, and are valid both when the hidden sector parameters are real and (at tree-level) complex.

3 To and From the Hidden Valley

Hidden sector states can be produced directly through their induced couplings to charged SM particles [18–21], from rare decays of the Z [10, 11], and at the end of MSSM cascades [3, 6]. The rates for the first two of these channels are suppressed by at least a factor of ϵ^2, but no such suppression is present for production via the MSSM. MSSM superpartner production can therefore be the dominant source of hidden states at high energy colliders, and we will focus exclusively on it in the present work.

With R-parity, R-odd MSSM superpartners are produced in pairs with full gauge strength and decay in a cascade down to the lightest MSSM superpartner. This would-be LSP is unstable, and can decay to the lighter hidden

states through the kinetic mixing coupling. The decay cascade continues in the hidden sector, possibly producing some R-even hidden states along the way. In turn, these can decay back to the SM through kinetic mixing interactions. The fact that we can both enter and leave the hidden sector through the same supersymmetric operator is a particular elegance of this model.

In this section we discuss the production of hidden states from MSSM decay cascades along with decays from the hidden sector back to the SM. We also classify the general structure of supersymmetric events at the Tevatron and the LHC in the presence of the minimal light hidden sector.

3.1 (MSSM) Decays Into the Hidden Sector

All of the MSSM superpartners can decay into the hidden sector. However, the partial widths are proportional to ϵ^2, and can usually be ignored for all fields other than the lightest SM superpartner (LSMP), which has no other decays open to it. The most important coupling for LSMP decays generally comes from the $U(1)_x$ gaugino interactions:

$$\begin{aligned} -\mathcal{L} &\supset \sqrt{2}\, g_x \big(H^* \tilde{H} \tilde{X} - H'^* \tilde{H}' \tilde{X}\big) \\ &\to \sqrt{2}\, g_x \big(H^* \tilde{H} \tilde{X} - H'^* \tilde{H}' \tilde{X}\big) - \epsilon \sqrt{2}\, g_x \big(H^* \tilde{H} \tilde{B} - H'^* \tilde{H}' \tilde{B}\big). \end{aligned} \tag{18}$$

Note that since the LSMP is unstable, the usual dark matter constraints do not apply and in particular, it need not be a neutralino. This divides supersymmetric hidden valley theories into four subclasses depending on the nature of the LSMP: a gluino, a sfermion, a neutralino, or an approximately degenerate chargino-neutralino pair (the structure of the MSSM mass matrix makes a LSMP chargino difficult to obtain [22]).

A gluino LSMP decays primarily through a four-body mode involving an off-shell squark and an off-shell neutralino, or in a three-body mode with an off-shell squark that relies on hidden-MSSM neutralino mass mixing. In both cases, two energetic quark jets are produced together with one or two hidden states. These decays can be prompt or significantly displaced, depending on the spectrum. For $m_{\chi^0} \sim m_{\tilde{q}} \gg m_{LSMP}$ there is a very strong kinematic suppression that can lead to a long-lived gluino and R-hadron-like signals [23].

The case of a sfermion LSMP was considered in Ref. [10]. It can decay in a three-body mode to the corresponding fermion and a pair of hidden states via an off-shell Bino, or in a two-body channel from mass mixing (induced by kinetic mixing) between the visible and hidden neutralinos. Both channels

can be comparable in rate, and are typically prompt unless there is additional suppression from kinematics or a very small value of the kinetic mixing. In particular, the kinematic suppression becomes severe if the sfermion is much lighter than the MSSM neutralinos [10].

A light chargino has some similarities to a sfermion; it can decay into the hidden sector to W/Higgs plus either two hidden states through an off-shell Bino, or one through the neutralino mass mixing. The chargino can also usually decay to the LSMP neutralino plus a pion [22]; since the pion is soft, it usually escapes detection and so this has the same collider signal as for the neutralino. All three chargino decays are prompt, and which dominates depends on the mass splitting with the neutralino.

In the present work we will focus on the third case where the LSMP is a neutralino. The interaction of Eq. (18) induces direct two-body decays to a hidden sector fermion and scalar (or vector). The total associated decay width is

$$\begin{aligned}\Gamma &= \frac{1}{8\pi} g_x^2 \epsilon^2 |N_{11}^*|^2 m_{LSMP} \\ &\simeq (2\times 10^{-18}\mathrm{s})^{-1} |N_{11}|^2 \left(\frac{g_x}{0.3}\right)^2 \left(\frac{\epsilon}{10^{-3}}\right)^2 \left(\frac{m_{LSMP}}{100\ \mathrm{GeV}}\right),\end{aligned} \tag{19}$$

where $|N_{11}|$ is the Bino fraction of the LSMP neutralino. These decays are prompt for parameter values remotely close to the fiducial values quoted here.

Decays of a neutralino LSMP to a hidden neutralino and a scalar (h_1^x, h_2^x, A^x) arise in an obvious way from the interactions of Eq. (18). Decays to the vector are also expected from the Goldstone equivalence principle [10], although their origin is a bit murkier in the unitary gauge (which we use here) where the Goldstone mode does not appear explicitly. In this gauge, the vector decay mode arises from the small mass mixing between the Bino and the hidden Higgsinos induced by the interaction of Eq. (18). The corresponding mixing angle goes like $(\epsilon\, m_x/m_{\chi_1^0}) \ll \epsilon$, but the mass suppression in this angle is cancelled in the squared matrix element by the kinematic enhancement of the coupling to the longitudinal mode of the vector that arises for $m_x \ll m_{\chi_1^0}$, as expected from the Goldstone boson equivalence theorem [24].

The Goldstone equivalence theorem also implies that the decays of the LSMP neutralino should populate the scalar and vector channels equally, up to kinematic effects. Explicitly, we find (neglecting the kinematic effects of

the hidden masses) the decay widths

$$\Gamma(\chi_1^0 \to \chi_j^x S^x) = \epsilon^2 \frac{g_x^2 m_{\chi_1^0} |N_{11}|^2}{32\pi} \times \begin{cases} \left|s_\zeta P_{j1}^* + c_\zeta P_{j2}^*\right|^2 & \text{if } S^x = X_\mu\,, \\ \left|c_\zeta P_{j1}^* - s_\zeta P_{j2}^*\right|^2 & \text{if } S^x = A^x\,, \\ \left|R_{11} P_{j1}^* + R_{12} P_{j2}^*\right|^2 & \text{if } S^x = h_1^x\,, \\ \left|R_{12} P_{j1}^* - R_{11} P_{j2}^*\right|^2 & \text{if } S^x = h_2^x\,. \end{cases} \tag{20}$$

Taking $S^x = A^x$ (for example) and summing over the hidden fermion flavours, we find

$$\begin{aligned} \sum_j \Gamma(\chi_1^0 \to \chi_j^x A^x) &= \epsilon^2 \frac{g_x^2 m_{\chi_1^0} |N_{11}|^2}{32\pi} \\ &\qquad \times \sum_j \Big[c_\zeta^2 P_{j1}^* P_{j1} + s_\zeta^2 P_{j2}^* P_{j2} - 2 s_\zeta c_\zeta Re(P_{j1}^* P_{j2}) \Big] \\ &= \epsilon^2 \frac{g_x^2 m_{\chi_1^0} |N_{11}|^2}{32\pi}\,, \end{aligned} \tag{21}$$

where we have used the unitarity of P in the last line. It is clear that the same result holds for the CP-even scalars as well as the vector, and even holds when the hidden sector breaks CP. In contrast, the relative decay widths to the hidden neutralinos are not democratic. It is clear from Eq. (18) that the mostly-Higgsino states will be preferred; summing over the scalar channels in Eq. (20) and using orthogonality of R, we find that

$$\sum_{S^x} \Gamma(\chi_1^0 \to \chi_j^x S^x) = \epsilon^2 \frac{g_x^2 m_{\chi_1^0} |N_{11}|^2}{16\pi} \left(|P_{j1}|^2 + |P_{j2}|^2 \right). \tag{22}$$

In particular, in the limit that the mass and gauge bases overlap, the LSMP will decay to the two Higgsinos with equal probability (and the gaugino not at all).

3.2 Decays Out of the Hidden Sector

All of the hidden states are electrically neutral and uncoloured, and are not directly visible at the LHC. Nevertheless, hidden particles can contribute more than just missing energy to collider events if they decay back to the SM. The only applicable coupling to induce such a decay is the gauge kinetic

mixing. We show here that this can allow the vector X_μ and the lightest scalar h_1^x to decay primarily to the SM to produce new observable effects in collider detectors, while the remaining hidden states decay almost entirely to other (possibly off-shell) hidden states.

Starting with the vector X_μ, its decays to the SM proceed at the rate [19, 21]

$$\Gamma(X \to SM) = \Gamma(X \to \ hadrons) + \sum_{\ell=e,\mu,\tau} \Gamma(X \to \ell\bar{\ell}) \tag{23}$$

where

$$\begin{aligned}\Gamma(X \to \ell\bar{\ell}) &= \frac{\epsilon^2\, c_W^2 g_x^2}{12\pi} m_x \sqrt{1 - \frac{4m_\ell^2}{m_x^2}} \left(1 + \frac{2m_\ell^2}{m_x^2}\right) \\ &\simeq (1.1 \times 10^{-5}\text{cm})^{-1} \left(\frac{\epsilon}{10^{-3}}\right)^2 \left(\frac{g_x}{0.3}\right)^2 \left(\frac{m_x}{1\text{ GeV}}\right), \end{aligned} \tag{24}$$

and

$$\Gamma(X \to \ hadrons) = \Gamma(X \to \mu^+\mu^-)\, R(s = m_x^2)\,, \tag{25}$$

with $R(s) = \sigma(e^+e^- \to hadrons)/\sigma(e^+e^- \to \mu^+\mu^-)$, measured values of which are tabulated in Ref. [25]. These decay modes typically only dominate the width of X_μ when all the possible two-body hidden decay channels, $X_\mu \to A^x h_1^x$ and $X_\mu \to \chi_i^x \chi_j^x$, are kinematically forbidden. On the other hand, if the vector can only decay to the SM, it is apt to be a rich source of additional fermions in supersymmetric collider events.

The lightest hidden scalar h_1^x can decay to the SM through its gauge-induced coupling to the vector X_μ and its mass mixing with the CP-even MSSM Higgs bosons. Both contributions to the total width are small relative to the mass, and usually relevant only when all the possible two-body hidden decays, $h_{1x} \to \chi_i^x \chi_j^x$, are kinematically forbidden. Even if the h_1^x mode decays exclusively to the SM, its lifetime can be so long that it decays far outside a typical collider detector and contributes only missing energy to collider events.

The long lifetime of h_1^x in the minimal model under consideration arises because it is constrained by the structure of the hidden sector to be lighter than the X_μ vector. As such, the only vector-induced decays of this light scalar are a four-body mode with two off-shell vectors, and a loop-mediated decay containing the vector [21]. In both cases the corresponding decay rates are proportional to ϵ^4, and are each too slow to allow the h_1^x to decay within the LHC (or Tevatron) detectors.

Mixing with the MSSM Higgs bosons by way of D-term interactions (listed in Appendix A, see Eq. (45)) also contributes to the decay width of h_1^x. The inclusive decay rate produced by this mixing is (in the MSSM Higgs decoupling limit)

$$\begin{aligned}\Gamma_{h_1^x} &= \epsilon^2 s_W^2 \left(\frac{m_x m_Z}{m_{h^0}^2}\right)^2 (s_\zeta R_{1a} + c_\zeta R_{2a})^2 \Gamma_{h^0}(m_{h_1^x}) \\ &\simeq (7.8\times 10^{-12})\,\Gamma_{h^0}(m_{h_1^x}) \\ &\quad\times\ (s_\zeta R_{1a} + c_\zeta R_{2a})^2 \left(\frac{\epsilon}{10^{-3}}\right)^2 \left(\frac{m_x}{\text{GeV}}\right)^2 \left(\frac{125\ \text{GeV}}{m_{h^0}}\right)^4 ,\end{aligned} \tag{26}$$

where $\Gamma_{h^0}(m_{h_1^x})$ is the decay width of a SM Higgs boson with mass equal to that of h_1^x. For h_1^x masses above the two-muon threshold, these Higgs-mixing decays dominate over those induced by the hidden vector. We illustrate the relative values of the decay length $c\tau$ for both decay mechanisms (considered individually) in Fig. 1 for $\epsilon = 10^{-3}$, $m_x = 1.5\, m_{h_1^x}$, $(s_\zeta R_{1a} + c_\zeta R_{2a})^2 = 1$, and $m_{h^0} = 125$ GeV. Note that the partial width to light hadrons includes the effects of hadronic form factors from Ref. [26], relevant in the region $2m_\pi \lesssim m_{h_1^x} \lesssim 1$ GeV. The total width accounts for (destructive) interference between the two contributions. From this figure, we see that the h_1^x state is stable on collider time scales for $m_{h_1^x} \lesssim 1$ GeV. In the present work we will focus on a range of hidden sector parameters for which the h_1^x state is very long-lived, either due to a small mass or from additional suppression due to mixing or kinematics. However, for larger masses the decays of h_1^x to heavy flavours may be visible in the LHC detector, a signal that is similar to those discussed for hidden valley models in Ref. [27].

The heavier hidden scalars typically decay much more efficiently within the hidden sector than to the SM. They can still contribute to visible collider objects if they decay to one or two vectors:

$$A^x \to h_1^x X_\mu; \quad h_2^x \to 2X_\mu; \quad h_2^x \to A^x X_\mu. \tag{27}$$

Note that in the last decay one of the final states is always virtual. These states may also decay to hidden neutralinos or multiple light scalars (for h_2^x). In all cases, the decays are typically prompt unless the mass spectrum forces them to go far off-shell.

Had we allowed violation of CP in the hidden sector, several new bosonic decays could become possible. Of these, two are potentially relevant:

$$A^x \to X_\mu X_\nu; \quad A^x \to h_1^x h_x^1\ . \tag{28}$$

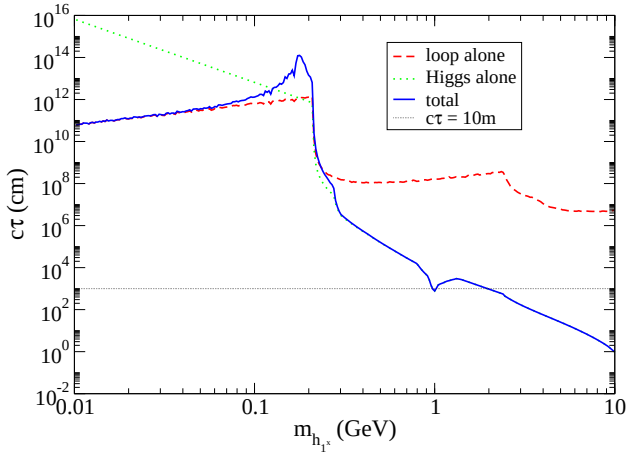

Figure 1: Decay length ($c\tau$) of the lightest hidden Higgs boson h_1^x for different decay mechanisms. In making this figure we have fixed $\epsilon = 10^{-3}$, $m_x = 1.5\, m_{h_1^x}$, $(s_\zeta R_{1a} + c_\zeta R_{2a})^2 = 1$, and $m_{h^0} = 125$ GeV. The horizontal dotted line corresponds to $c\tau = 10\,\mathrm{m}$, roughly the radius of the LHC detectors.

These decays are suppressed compared to the CP-conserving ones by the small A^x–$h^x_{1,2}$ mixing, but can be important in particular regions of parameter space. The former decay is enhanced when $m_{A^x} \gg m_x$ by the coupling to the longitudinal mode of the vector. It is unlikely to be relevant for the parameter space we consider, since we assume no large mass hierarchies in the hidden sector. The decay to two scalars can be relevant when no other hidden sector decays of A^x are open. In this case, the leading mode in the CP-conserving case is to the SM through an off-shell vector. Whether the CP-violating decay can dominate this depends on the precise spectrum and the size of the A^x–h^x_2 mixing, which are model dependent qualities. It is a model-independent statement that this decay mode will lead to fewer decays back to the visible sector (and thus more missing energy).

By R-parity, the fermion decay modes all have the form

$$\chi_i^x \to \chi_j^x S^{x\,(*)} \quad (i > j)\,, \tag{29}$$

where $S^x = h_1^x$, h_2^x, A^x, X_μ, and the bosonic product may be off-shell. In particular, if the $\chi_1^x\, h_1^x$ final state is forbidden, the dominant decay mode will normally be through an off-shell vector. Calculating the width for this

process requires an integration over the hidden vector width:

$$\Gamma = \frac{|G_{ij}|^2 \left|m_{\chi_i^x}\right|}{16\pi} \int dQ^2 \, \frac{m_{\chi_i^x}^2}{Q^2} \, \frac{\sqrt{Q^2}\,\Gamma(X \to SM; m_x = \sqrt{Q^2})}{(Q^2 - m_x^2)^2 + m_x^2\Gamma_x^2} \times \sqrt{I(\rho_1, \rho_2)} \left[(1-\rho_1^2)^2 + \rho_2^2(1+\rho_1^2) - 2\rho_2^4 + 6\rho_2^2 \frac{\Re(G_{ij}^2)}{|G_{ij}|^2} \right], \quad (30)$$

where

$$\rho_1 = \frac{m_{\chi_j^x}}{m_{\chi_i^x}}, \quad \rho_2 = \frac{\sqrt{Q^2}}{m_{\chi_i^x}}, \quad (31)$$

the coupling G_{ij} is

$$G_{ij} = g_x(P_{i1}P_{j1}^* - P_{i2}P_{j2}^*), \quad (32)$$

and the phase space function

$$I(a,b) = 1 - 2a^2 - 2b^2 + a^4 + b^4 - 2a^2b^2. \quad (33)$$

Note that unless the fermion mass splitting is less than $2m_\pi$, this requires an integration over the experimentally-measured function $R(s)$, defined below Eq. (25). If the fermion mass splitting is less than $2m_e$, the decay will instead proceed through an off-shell h_1^x to $\chi_1^x\gamma\gamma$. As for the heavier fermions, these decays are prompt unless they are limited by kinematics. The presence of CP violation would change the branching fractions for these modes, but lead to no new decays.

In summary, the only significant exit channels from the hidden sector are through the vector X_μ or the lightest scalar h_1^x, with the latter occurring too late to be seen in typical colliders for the parameter ranges to be considered in the present work. Hidden vectors can be created directly from the LSMP decay, as well as from cascade decays within the hidden sector. Additional vectors can also be produced from hidden showering as discussed in Refs. [11–14]. Once a hidden vector is created, it will decay back to the SM provided it has no open channels within the hidden sector. Indeed, this condition is close to a necessary one for the hidden sector to contribute more than just missing energy in high-energy collisions.

3.3 Collider Events

Putting together the pieces from the discussion above, a simple picture emerges for supersymmetric events at high-energy colliders. MSSM superpartners are produced in pairs and decay in a cascade down to the LSMP.

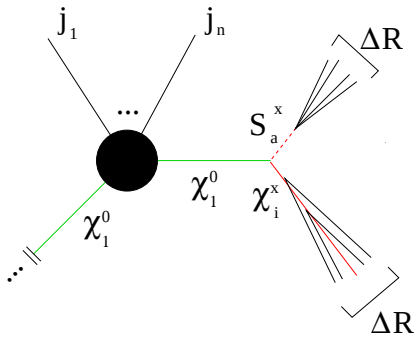

Figure 2: Schematic overview of an HV collider event.

These decay subsequently to a hidden fermion and a hidden boson. The cascade continues within the hidden sector, and some hidden vectors may be produced along the way. If the vector decays back to the SM, the MSSM cascade will be accompanied by additional SM particles as well missing energy from the stable or long-lived hidden states.

Since the MSSM LSMP is assumed to be much heavier than any of the states in the hidden sector, the two decay products of the LSMP will each be highly boosted by an amount $\gamma \sim m_{LSMP}/m_{hid}$. On each branch, the cascade will continue, and any further decay products will be collimated by an amount $\Delta R \sim 1/\gamma$. In particular, a vector created along the way will produce a highly collimated hadronic jet, or a *lepton jet* consisting of two or more collimated leptons with possible additional hadronic activity [6, 10, 11]. The branching ratios of the vector follow from Eq. (23). We will refer to these highly collimated objects together as HV jets.

We can classify supersymmetric events in this scenario by the number of HV jets they contain together with the structure of the HV jets themselves. We illustrate the situation schematically in Fig. 2. Each LSMP can produce zero, one, or two HV jets, and there are two LSMPs per event. A given HV jet can be prompt, leaving visible tracks directly from the interaction vertex, or displaced, with visible tracks beginning only after a macroscopic distance. An HV jet may also contain the decay products of more than one vector, yielding additional substructure within the single collimated detector object.

Thus, we have

$$\left\{ \text{ MSSM cascade } \right\} \ \oplus \ \left\{ \begin{array}{l} \text{0 HV jets} \\ \text{1 HV jets} \\ \text{2 HV jets} \\ \text{3 HV jets} \\ \text{4 HV jets} \end{array} \right. \ \otimes \ \left. \begin{array}{l} \text{prompt track} \\ \text{delayed track} \end{array} \right\} \tag{34}$$

We will show below that many of these possibilities can occur in different events derived from a single set of hidden sector parameters.

4 Hidden Sector Parameter Scan

As discussed above, the collider signals of a supersymmetric hidden sector depend on two main quantities: the number HV jets produced per LSMP decay to the hidden sector; and whether or not there are any long-lived hidden states that produce displaced vertices. To investigate the full range of collider signals (for a neutralino LSMP) and to see how they depend on the hidden sector parameter values, we have implemented this model in FeynRules 1.4.9 [28] and MadGraph 4.4.49 [29]. We have computed decay tables for the LSMP neutralino and hidden sector particles using numerical evaluation of the analytic (tree-level) expressions. In particular, the decays to the visible sector used the experimentally measured ratio R as described in Eqs. (23), (25) and (30). For decays to the hidden sector, we have checked our results against BRIDGE 2.23 [30].

The parameter space of the hidden sector can be described uniquely by seven independent parameters (once the spontaneous breakdown of $U(1)_x$ is imposed). We have chosen to use the set $\{m_x,\, m_{A^x},\, M_x,\, \mu',\, \tan\zeta,\, g_x,\, \epsilon\}$. We then generated 2×10^4 points in this parameter space, fixing $g_x = 0.3$ and $\epsilon = 10^{-3}$, but otherwise scanning over the ranges listed in Table 1. These values are generally consistent with direct low-energy searches for light hidden sectors [19,20,31,32]. All magnitudes were selected using logarithmic priors, while the two signs of μ' were equally probable. We also took the LSMP to be a mostly-Bino neutralino with a mass of 300 GeV. Similar results are expected for mostly Wino or Higgsino neutralino LSMP provided it has a significant Bino fraction.

Parameter	Range
m_x	(0.1, 10) GeV
m_{A^x}	(0.1, 10) GeV
M_x	(0.1, 10) GeV
μ'	$\pm$ (0.1, 10) GeV
$\tan\zeta$	(0.1, 10)

Table 1: Range of Hidden Sector parameters considered in the scan.

4.1 Number of HV Jets

The first set of quantities of interest are the probabilities $\tilde{\mathcal{P}}_{\tilde{N}}$ for an LSMP neutralino to produce $\tilde{N} = 0, 1, 2$ HV jets. Additional HV jets can arise from hidden sector radiation, but we do not consider this effect here since it is expected to be very mild for the value of $g_x = 0.3$ we are using [11–13]. Furthermore, for the ranges of hidden sector parameters used in our scan we find that the h_1^x scalar is almost always effectively stable on collider scales, either because it is light or due to small mixing angles or a large boost. The exceptions comprise $\mathcal{O}(0.1\%)$ of our scan; apart from these points, the only source of HV jets for this range of parameters is therefore the hidden vector X^μ.

Before addressing the probabilities $\tilde{\mathcal{P}}_{\tilde{N}}$ directly, it is instructive to first discuss the two closely-related quantities $\mathcal{P}_F$ and $\mathcal{P}_B$. They are defined to be the probabilities of an HV jet being produced in the hidden sector cascades initiated by the fermion or the boson decay product of the (neutralino) LSMP, averaged over all LSMP decay modes and weighted by the relevant branching fractions. They are calculated using the hidden and LSMP decay tables and lengths, specifically by replacing particles by their decay tables till either an HV jet or a collider-stable particle is produced. Our working definition of "collider-stable" for this study is a (boosted) decay length greater than $\gamma c\tau > 10\,\mathrm{m}$, where we estimate the boosts of the hidden states by assuming that they are produced with an energy of $m_{LSMP}/2 = 150$ GeV.

In Fig. 3 we show the distribution of values of $\mathcal{P}_B$ and $\mathcal{P}_F$ found in our parameter scan. Several features are clearly visible in this plot. In particular, there are agglomerations of points for: i) $\mathcal{P}_B = 0.25$, 0.5 and 0.75, with various values of $\mathcal{P}_F$; ii) $\mathcal{P}_F = 0.0$ and 0.5, for various values of $\mathcal{P}_B$; and iii) for $\mathcal{P}_F = \mathcal{P}_B$. There is also a less-obvious but significant feature at $\mathcal{P}_B, \mathcal{P}_F \approx 0$ that includes over 40% of the points in our scan. These features

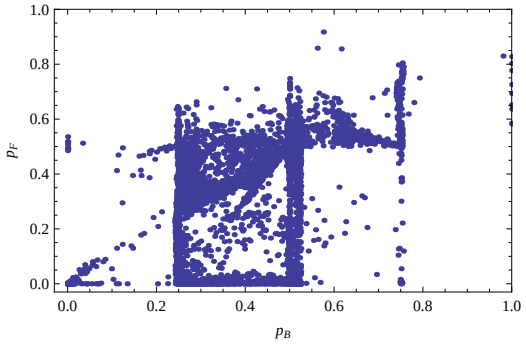

Figure 3: The distribution of values of $\mathcal{P}_B$ and $\mathcal{P}_F$ found in our parameter scan over the hidden sector. Each point in the plot corresponds to a single point in the parameter scan, but it is possible for points to overlap at this resolution.

can be understood in terms of the hidden sector spectrum, with mixing effects subdominant.

The agglomerated values of $\mathcal{P}_B$ are most easily understood in terms of the result of Eq. (21), that the LSMP decays to each hidden sector boson with equal frequency. This implies that the points for which $\mathcal{P}_B = 0$ (0.25, 0.5, 0.75) are those where none (one, two, three) hidden bosons decay visibly and the rest invisibly (*i.e.* outside the detector or to other invisible states). There are very few points with $\mathcal{P}_B \gtrsim 0.8$ due to h_1^x; as discussed in Sec. 3.2, direct decays of this state to the SM are normally too slow to occur inside the detector.

The points in Fig. 3 with small values of both $\mathcal{P}_B$ and $\mathcal{P}_F$ are necessarily those where the X^μ gauge boson has on-shell decays to other hidden states. However, the converse is not true. In Fig. 4 we show $\mathcal{P}_B$ and $\mathcal{P}_F$ for those points in our scan where the decay $X_\mu \to A^x h_1^x$ is allowed, which is almost always the most important hidden mode. Non-zero values of $\mathcal{P}_B$ still arise in this case when the pseudoscalar decays sufficiently promptly to an off-shell gauge boson whose invariant mass is too small to decay invisibly. When $\mathcal{P}_B$ is small, $\mathcal{P}_F$ will usually also be small as the fermions can only decay to hidden sector bosons. The exception occurs when χ_2^x has no two-body decays, and will be discussed in more detail below.

When the X_μ vector boson does decay mainly to the SM, we find $\mathcal{P}_B \geq 0.25$. Even larger values of $\mathcal{P}_B$ can come about when the other bosons produce

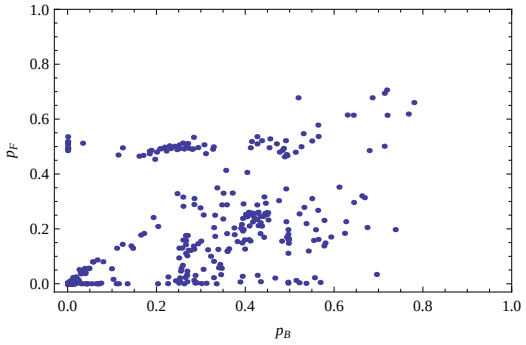

Figure 4: The distribution of values of $\mathcal{P}_B$ and $\mathcal{P}_F$ from Fig. 3, restricted to those points where the decay $X_\mu \to A^x h_1^x$ is kinematically allowed. Most points in this plot are at $\mathcal{P}_B, \mathcal{P}_F \approx 0$ and overlap at this resolution.

vectors in their decay chains. For the pseudoscalar A^x, if it has no fermion decay modes it must decay to either a real or virtual X_μ, which will typically be visible unless it is far off-shell. Neglecting subsequent fermion decays, the A^x state thus contributes

$$\mathcal{P}_B(A^x) \simeq 0.25 \times \left[1 - \sum_{i \geq j} \mathrm{BR}(A_x \to \chi_i^x \chi_j^x)\right] . \tag{35}$$

In contrast, the heaviest boson h_2^x generically contributes little to $\mathcal{P}_B$; even if it has no fermionic decays, the decay to $2h_1^x$ will usually dominate the decays to vectors if it is allowed.[4] In particular, the points with $\mathcal{P}_B \gtrsim 0.5$ require a highly compressed spectrum: $m_{h_1^x} < m_{A^x}, m_x < m_{h_2^x} < 2m_{h_1^x}$, or in terms of our input parameters $m_{A^x}/2 < m_x < 2m_{A^x}$ and $0.5 < \tan\zeta < 2$.

Turning next to the fermion side, the agglomerations of points at $\mathcal{P}_F \simeq 0, 0.5$ can arise in several different ways. First of these is when $m_x < |\mu'| \ll M_x$, leading to a spectrum with two light, nearly-degenerate Higgsino-like χ_1^x, χ_2^x states and a more massive gaugino-like χ_3^x. The LSMP will then decay to χ_1^x and χ_2^x with nearly equal frequency (see Eq. (22)) and to χ_3^x very rarely. The mass splitting of the Higgsino-like $\chi_{1,2}^x$ pair is roughly $m_x^2/|\mu'| < m_x$, so χ_2^x decays exclusively to either the invisible h_1^x or an off-shell vector. The former leads to $\mathcal{P}_F \simeq 0$; the latter to $\mathcal{P}_F \simeq 0$ or 0.5, depending on whether

[4]Note as well that the decay $h_2^x \to A^x X_\mu$ is never on shell, and if the decay $h_2^x \to 2X_\mu$ is open we are in the decoupling limit where the scalar decay dominates.

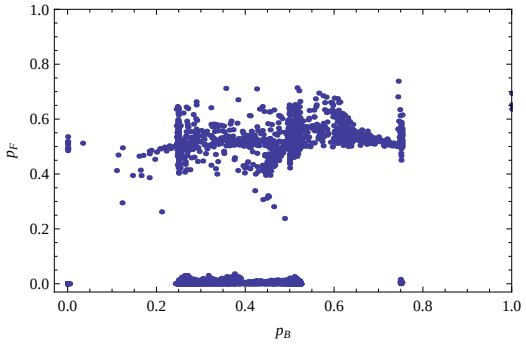

Figure 5: The distribution of values of $\mathcal{P}_B$ and $\mathcal{P}_F$ in our scan restricted to those points where the decay $\chi_2^x \to h_1^x \chi_1^x$ is *not* kinematically allowed. The points with $\mathcal{P}_F \approx 0.5$ (0) are those where the χ_2^x decays inside (outside) the detector.

the decay occurs inside the detector. This behaviour can be seen clearly in Fig. 5 where we show the values of $\mathcal{P}_B$ and $\mathcal{P}_F$ for those points where $\chi_2^x \to h_1^x \chi_1^x$ is not kinematically possible.

Values of $\mathcal{P}_F \simeq 0.5$ can also arise when $M_x \ll |\mu'|$ and $m_x \lesssim |\mu'| \lesssim m_{A^x}$. In this case, the Higgsino-like states are the more massive fermions χ_2^x and χ_3^x, and they decay to the gaugino-like χ_1^x and either X_μ or h_1^x exclusively. While the branching ratios for one Higgsino to these two final states may be unequal, generically the other Higgsino has a complementary decay pattern. The result is that the rates for $\chi_1^0 \to \chi_{2,3}^x \to S^x \chi_1^x$ are equal for $S^x = X_\mu, h_1^x$, leading to $\mathcal{P}_F \simeq 0.5$. This feature is illustrated in Fig. 6, where we show the values of $\mathcal{P}_B$ and $\mathcal{P}_F$ for those points where $\chi_2^x \to X_\mu \chi_1^x$ is kinematically allowed but $\chi_3^x \to A^x \chi_1^x$ is not.

In Fig. 3 we also see an agglomeration of points with $\mathcal{P}_F \sim \mathcal{P}_B$. This typically occurs when the Higgsino-like fermions are somewhat heavy and can decay to all scalars. The fermionic side of the LSMP decay chain then proceeds according to $\chi_1^0 \to \chi_{2,3}^x S^x$, followed by $\chi_{2,3}^x \to \chi_1^x S^{x\prime}$ with roughly equal probability for all four bosonic final states $S^{x\prime}$. Thus, the distribution of bosons produced in the decays of $\chi_{2,3}^x$ in this case mirrors those of the neutralino LSMP giving $\mathcal{P}_B \sim \mathcal{P}_F$. We illustrate this behaviour in Fig. 7, where we show in black the values of $\mathcal{P}_B$ and $\mathcal{P}_F$ for those points where $\chi_2^x \to \chi_1^x(X_\mu,\ h_1^x,\ A^x,\ h_2^x)$ are all allowed. The additional agglomerations of points in Fig. 7 extending away from the $\mathcal{P}_F \simeq \mathcal{P}_B$ line correspond to

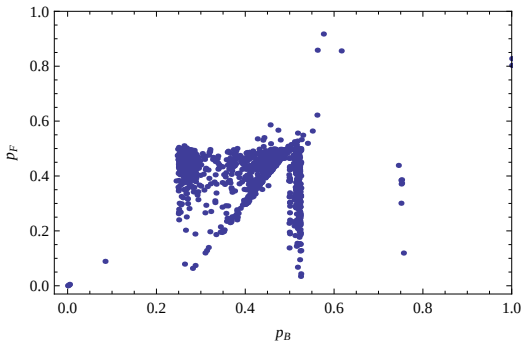

Figure 6: The distribution of values of $\mathcal{P}_B$ and $\mathcal{P}_F$ in our scan restricted to those points where the decay $\chi_2^x \to X_\mu \chi_1^x$ is kinematically allowed and the decay $\chi_3^x \to A^x \chi_1^x$ is not.

parameter values that lead to all fermions being heavier than the bosons but also well-mixed. In Fig. 7 we also show in red those points where $\chi_2^x \to \chi_1^x X^\mu$ and $\chi_2^x \to \chi_1^x A^x$ are allowed but $\chi_2^x \to \chi_1^x h_2^x$ is not. These points have nearly the same structure as those where all three boson modes are open since, as discussed above, the decays of h_2^x are typically invisible.

The probabilities $\mathcal{P}_{B,F}$ are related to the probabilities $\tilde{\mathcal{P}}_{\tilde{N}}$ that a LSMP neutralino decay will produce $\tilde{N} = 0-2$ HV jets:

$$\tilde{\mathcal{P}}_0 = 1 - \mathcal{P}_B - \mathcal{P}_F + (\mathcal{P}_B \mathcal{P}_F - \mathcal{C}) \ , \tag{36}$$

$$\tilde{\mathcal{P}}_1 = \mathcal{P}_B + \mathcal{P}_F - 2(\mathcal{P}_B \mathcal{P}_F - \mathcal{C}) \ , \tag{37}$$

$$\tilde{\mathcal{P}}_2 = \mathcal{P}_B \mathcal{P}_F - \mathcal{C} \ , \tag{38}$$

where $\mathcal{C}$ describes the degree of correlation between $\mathcal{P}_B$ and $\mathcal{P}_F$ (with Eq. (38) as its defining relation). In particular, if $\mathcal{P}_B$ and $\mathcal{P}_F$ were independent, $\mathcal{C}$ would vanish. In Fig. 8 we show the values of the correlation coefficient $\mathcal{C}$ relative to $\mathcal{P}_B$ and $\mathcal{P}_F$.

By R-parity, each supersymmetric event will involve two neutralino LSMPs. Since the two LSMP decays in an event are independent, it is trivial to relate the values of $\tilde{\mathcal{P}}_{\tilde{N}}$ to the probabilities P_N for an event to have $N = 0-4$ HV jets.[5] Based on our previous results, we can identify three qualitative behaviours:

[5] To wit: $P_0 = \tilde{\mathcal{P}}_0^2$, $P_1 = 2\tilde{\mathcal{P}}_0\tilde{\mathcal{P}}_1$, $P_2 = \tilde{\mathcal{P}}_1^2 + 2\tilde{\mathcal{P}}_0\tilde{\mathcal{P}}_2$, $P_3 = 2\tilde{\mathcal{P}}_1\tilde{\mathcal{P}}_2$, $P_4 = \tilde{\mathcal{P}}_2^2$.

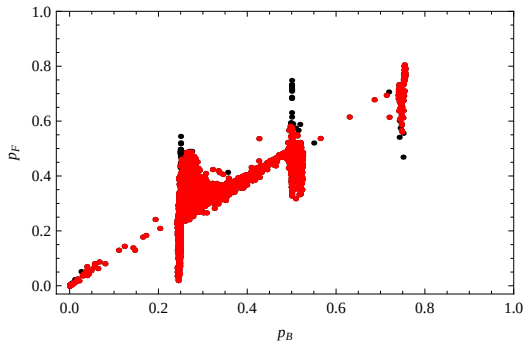

Figure 7: The distribution of values of $\mathcal{P}_B$ and $\mathcal{P}_F$ obtained in our scan restricted to those points where the decays $\chi_2^x \to X_\mu \chi_1^x$ and $\chi_2^x \to A^x \chi_1^x$ are kinematically allowed. The points in black (red) are those where the decay $\chi_2^x \to h_2^x \chi_1^x$ is (is not) allowed.

- Small $\mathcal{P}_B$ and $\mathcal{P}_F$, with the number of HV jets peaked at $N = 0-1$;
- Large $\mathcal{P}_B$ and $\mathcal{P}_F$, with the number of HV jets peaked at $N = 3-4$;
- Intermediate cases, with the number of HV jets peaked around $N = 2$.

In the last case, there is a further distinction between $\mathcal{P}_B \sim \mathcal{P}_F$, where the distribution in the number of HV jets is frequently broad; and $\mathcal{P}_B \gg \mathcal{P}_F$ or $\mathcal{P}_B \ll \mathcal{P}_F$, when the distribution is narrow. Considering the classification by decay mode discussed above, we note that approximately 40% of points with $\mathcal{P}_F, \mathcal{P}_B \simeq 0$ fall into the first category; most of the points with $\mathcal{P}_B \simeq 0.75$ fall into the second category; and the remaining points along the $\mathcal{P}_F \simeq \mathcal{P}_B$ line fall into the last category. The points with invisible fermions but moderate to large $\mathcal{P}_B$ also fall into the last category, but into the "narrow" subset.

4.2 Presence of Displaced Vertices

The other main phenomenological feature of the hidden sector is the presence or absence of displaced vertices. Our working definition of a displaced vertex is a decay from the hidden sector to the visible with a (boosted) decay length larger than $\gamma\, c\tau > 0.1\,\text{mm}$ but less than $\gamma\, c\tau = 10\,\text{m}$. This definition is crude, as the phenomenological implications depend in a very important way on the location in the detector the decay occurs. For example, it is much easier to

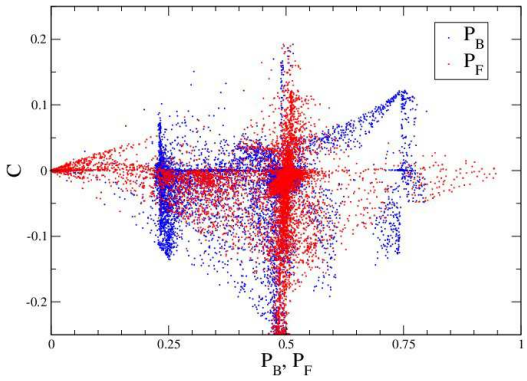

Figure 8: Values of $\tilde{\mathcal{P}}_B$ and $\tilde{\mathcal{P}}_F$ relative to the correlation coefficient $\mathcal{C}$.

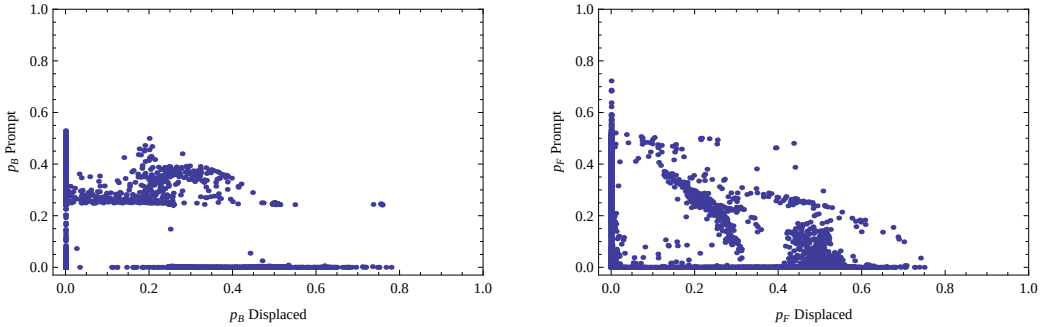

Figure 9: Relative frequencies of prompt and displaced decays for the bosonic (left) and fermionic (right) branches of LSMP neutralino decay cascades.

resolve a displaced vertex if the products are visible in the tracking chambers (corresponding to a true displaced vertex in the usual sense) [33]. We will mostly ignore this distinction in this section, but we shall discuss it in more detail in the next.

The relative probabilities for prompt and displaced vertices from the bosonic (fermionic) side of the decay chain are shown in the left (right) panel of Fig. 9. In particular, note that the sum of the two probabilities plotted equal $\mathcal{P}_B$ ($\mathcal{P}_F$). Both plots show concentrations of points along the axes where all decays are either prompt or displaced, as well as a numerically smaller set involving both types of decays.

For the moderate value of $\epsilon = 10^{-3}$ we are using, we find that displaced

vertices correspond to off-shell decays in the hidden sector. More precisely displaced vertices only occur if either A^x or χ_2^x have no two-body decays. We also find some points in our scan where h_2^x also decays off-shell, but the structure of the scalar potential means that for all such points the same is true for A^x. There are no points in our scan where χ_3^x has no two-body decays.

The points where all decays are displaced are the simplest to understand; they are almost exclusively the points (shown in Fig. 4) where the hidden vector can decay into the hidden sector. This is reasonable as in such a scenario the *only* significant decays from the hidden sector to the SM must be those where X_μ is off-shell. There are some additional points where the fermionic decays are all displaced that correspond to a subset of the points plotted in Fig. 5, where the only fermionic decays back to the SM are $\chi_2^x \to X_\mu^* \chi_1^x$. The set of points where all decays are prompt is also qualitatively simple, but involves a large number of different possible spectra and decay patterns. In essence, however, they correspond to points where all hidden sector particles either decay on-shell or are collider stable.

More interesting are the points with both prompt and displaced vertices. On the bosonic side, there are two obvious features in the left panel of Fig. 9. The line of points with $\mathcal{P}_B(\text{prompt}) \simeq 0.25$ are those where the hidden gauge boson decays promptly to the SM, while A^x and h_2^x have displaced off-shell decays, on-shell invisible decays, or decays to χ_2^x which in turn decays off-shell. Note that even when these heavier scalars can decay to the hidden vector, such modes are suppressed by mixing angles in the decoupling limit so that decays to fermions will typically dominate when they are open. The other main feature on the bosonic side are the points with $\mathcal{P}_B(\text{prompt}) > 0.25$. These also involve decays to a long-lived χ_2^x state, but now the heaviest fermion χ_3^x is also produced in scalar decays. It decays promptly, emitting vectors some fraction of the time. This last feature is more sensitive to the fermion mixing matrices, which is why the corresponding points form an amorphous blob instead of a line.

The fermionic decays that lead to both prompt and displaced vertices have a more complex structure, as can be seen in the right panel of Fig. 9. This structure decomposes into three parts. The first is a collection of points at $\mathcal{P}_F(\text{displaced}) \simeq 0.5$ that arise from off-shell χ_2^x and on-shell χ_3^x decays, though the latter are suppressed by small LSMP branching fractions. The second fermionic feature is the line of points where the prompt and displaced probabilities sum to about 0.5. This subset is characterised by off-shell A^x

	$\mathcal{P}_B$	$\mathcal{P}_F$	$\tilde{\mathcal{P}}_0$	$\tilde{\mathcal{P}}_1$	$\tilde{\mathcal{P}}_2$	$c\tau$(mm)
HV1	0.00	0.00	1.00	0.00	0.00	0.0
HV2	0.25	0.00	0.75	0.25	0.00	0.0
HV3	0.26	0.28	0.57	0.31	0.12	10.0
HV4	0.46	0.44	0.34	0.43	0.23	0.0
HV5	0.50	0.57	0.22	0.50	0.28	0.0, 0.2, 8.4

Table 2: Decay yields $\tilde{\mathcal{P}}_B$ and $\tilde{\mathcal{P}}_F$ and decay probabilities $\tilde{\mathcal{P}}_0$, $\tilde{\mathcal{P}}_1$, $\tilde{\mathcal{P}}_2$ from LSMP neutralino decays for all five sample points as well as the decay lengths $c\tau$ of any particles likely to lead to displaced vertices in high-energy collider events.

and on-shell h_2^x decays, plus heavier Higgsino-like fermions able to decay to all the bosons on-shell. The third feature in Fig. 9 are the two lines sloping between $\tilde{\mathcal{P}}_F$(prompt) and $\tilde{\mathcal{P}}_F$(displaced) from $(0.0, 0.5)$ to $(0.2, 0.4)$ and $(0.2, 0.8)$. These points have similar spectra to those of the second feature, except that now the heaviest scalar h_2^x is also constrained to decay through an off-shell gauge boson.

5 Sample Points

To further illustrate the diverse range of collider signals that can arise from this minimal HV theory, we present and investigate the properties of five distinct sample parameter points obtained in our scan. As in Section 4, we assumed a Bino-like neutralino LSMP of mass $m_{\chi_1^0} = 300$ GeV.

5.1 General Properties

In Table 2 we list the values of $\mathcal{P}_B$, $\mathcal{P}_F$, $\tilde{\mathcal{P}}_0$, $\tilde{\mathcal{P}}_1$, and $\tilde{\mathcal{P}}_2$ for all five sample points. We also list the characteristic decay lengths $c\tau$ of any long-lived particles likely to lead to displaced vertices. Note that since the LSMP is much heavier than the hidden sector states, the observed displacements will be greater by a factor $\gamma \sim m_{LSMP}/2m_{hid} \sim \mathcal{O}(50-100)$. In Table 3 we list the mass spectrum for the five benchmark points, and the underlying parameter input values are tabulated in Appendix B.

	m_x	$m_{h_1^x}$	$m_{h_2^x}$	m_{A^x}	$m_{\chi_1^x}$	$m_{\chi_2^x}$	$m_{\chi_3^x}$
HV1	5.73	0.57	5.73	0.60	1.91	9.28	9.50
HV2	0.65	0.06	7.46	7.43	0.57	1.09	1.34
HV3	6.49	1.95	7.40	4.04	2.07	6.42	7.28
HV4	0.90	0.67	9.74	9.72	0.48	1.93	2.12
HV5	3.54	1.82	4.26	3.00	1.97	3.70	10.14

Table 3: Particle masses in GeV for the sample points discussed in the text.

HV1 – Invisible

The first benchmark point HV1 is essentially invisible, with nearly all hidden sector cascades producing only states that are stable (χ_1^x) or very long-lived on collider timescales (h_1^x, A^x). The vector decays almost entirely invisibly via $X^\mu \to h_1^x A^x$ rather than to the SM ($BR \lesssim 10^{-6}$). The lighter two of the other bosonic states decay slowly through multi-body modes and are effectively stable on collider time scales, and the lightest fermion is stable and also invisible. The heaviest boson and the two heavier fermions decay to the invisible states, not the vector. Thus, the hidden states produced by the cascades just contribute to missing energy, and this theory is nearly indistinguishable from the MSSM at high-energy colliders.

HV2 – Visible Vectors

This point yields hidden cascades that are invisible except for when the vector X^μ arises directly in the LSMP decay. Once produced, the vector decays promptly and nearly entirely to the SM. The other particles are stable or long-lived, or decay to invisible states.

About one quarter of the LSMP neutralino decays produce a vector, yielding a probability distribution for the total number of HV jets in supersymmetric events of

$$P_0 = 0.56, \quad P_1 = 0.38, \quad P_2 = 0.06, \quad P_3 = 0, \quad P_4 = 0 \ .$$

We see that over half the supersymmetric events for this point reproduce the standard MSSM pattern of missing energy, and therefore the standard supersymmetry searches will be sensitive to the MSSM portion of this HV theory as well [33]. However, over a third of the supersymmetric events will also contain an additional HV jet beyond the standard MSSM cascade

products. Detecting and measuring such an object would give evidence for the existence of an additional hidden sector.

HV3 – Displaced Vertex

The third sample point has a more complicated decay pattern as well as a macroscopically displaced decay vertex. Both the boson and fermion sides of the LSMP decay chain can produce HV jets. On the bosonic side, visible HV jets come mainly from direct decays to the pseudoscalar followed by $A^x \to h_1^x X^{\mu *}$ with the off-shell vector going to the SM. This decay has a macroscopic lifetime of $c\tau = 10\,\text{mm}$ due to the vector being far off shell, but the actual decay length in collider events will be enhanced by a relativistic boost of $\gamma \sim m_{\chi_1^0}/m_{A^x} \sim \mathcal{O}(50)$. Similarly, HV jets are produced on the fermionic side from the A^x produced in the decays $\chi_{2,3}^x \to \chi_1^x A^x$.

In total, the distribution of HV jets in supersymmetric events is

$$P_0 = 0.32, \quad P_1 = 0.36, \quad P_2 = 0.23, \quad P_3 = 0.07, \quad P_4 = 0.01\ .$$

Again, a significant fraction of these events produce missing energy as in the MSSM, but the majority also have HV jets characterised by a displaced vertex.

HV4 – Multiple HV Jets

This sample point is very likely to produce additional HV jets. The vector X^μ decays promptly to the SM nearly all the time. In addition to direct production from the LSMP, vectors are frequently produced in the decays of the two Higgsino-like heavier fermions. The heavier scalars rarely decay directly to X^μ; instead they dominantly decay to fermions, producing HV jets through a multi-step decay chain.

The probability distribution for HV jets in supersymmetric events is

$$P_0 = 0.11, \quad P_1 = 0.29, \quad P_2 = 0.34, \quad P_3 = 0.20, \quad P_4 = 0.05\ .$$

In this case, only a small fraction of the collider events fall into the usual MSSM form.

HV5 – Multiple HV Jets and Displaced Vertices

Our fifth and last benchmark point produces many HV jets with both prompt and displaced decay vertices. The vector decays promptly to the SM almost

exclusively. The pseudoscalar decays mainly through $A^x \to h_1^x X^{\mu *}$ while the heavy scalar decays mostly invisibly via $h_2^x \to \chi_1^x \chi_1^x$. The pseudoscalar decay length is $c\tau = 8.4$ mm. On the fermionic branch of the LSMP decay, the two lighter Higgsino-like states are produced most abundantly. Of these, the decay of the heavier state $\chi_2^x \to \chi_1^x X^{\mu *}$ involves an off-shell vector and has a decay length of $c\tau = 0.2$ mm. Again, both the metastable states will be highly boosted when produced in LSMP decays, increasing the observed displacements.

The distribution of the number HV jets produced by MSSM collider events is

$$P_0 = 0.05, \quad P_1 = 0.22, \quad P_2 = 0.37, \quad P_3 = 0.28, \quad P_4 = 0.08 \; .$$

Only a small fraction of collider events will have no additional HV activity, while those events with HV jets can have both prompt and displaced decay vertices.

5.2 Structure of HV Jets

The basic structure of the HV jets arising for all the sample points is similar and relatively simple. In most cases, they come from the decay of a *single* hidden vector X^μ boosted by an amount $\gamma \simeq m_{\chi_1^0}/2m_1$, where m_1 is the mass of first boson or fermion produced in the LSMP neutralino decay chain that gives rise to the vector. The exception is HV4, where the two heavier scalars can decay to two vectors through intermediate fermions; however, even here the single vector channels are more common. As such, each HV jet is typically initiated by two hard objects collimated within a cone of size $\Delta R \lesssim \gamma\,(\sqrt{s_x}/m_1)$, where $\sqrt{s_x} \leq m_x$ is the invariant mass of the (possibly off-shell) decaying vector. More complicated HV jets containing the decay products of multiple vectors could arise if we took a larger coupling g_x to produce significant hidden vector showering.

The content of the HV jets depends on the value of $\sqrt{s_x}$ according to Eq. (23). We have $\sqrt{s_x} = m_x$ for on-shell decays (HV2, HV4, HV5); $\sqrt{s_x} \leq (m_{A^x} - m_{h_1^x})$ for off-shell pseudoscalar decays (HV3 and HV5); and $\sqrt{s_x} \leq (m_{\chi_2^x} - m_{\chi_1^x})$ for off-shell fermion decays (HV5).

Leptonic HV jets are the most promising collider signature of this class of supersymmetric hidden valleys. Their identification will likely require a dedicated search since the leptonic (e, μ) constituents are expected to be

nearly collinear and fall within a single typical lepton isolation cone ($\Delta R \leq 0.4$). Proposals for such searches have been made for the Tevatron [10,11,34, 35] and the LHC [10,11,36]. For example, Ref. [11] advocated a requirement of two or more leptons with $p_T > 10$ GeV collimated within a cone of $\Delta R < 0.1$ with an additional isolation cut of $\sum p_T < 3$ GeV in the surrounding region $0.1 < \Delta R < 0.4$.

This type of search is expected to be highly efficient for the prompt leptonic HV jets arising for HV2, HV4, and HV5, especially because they derive from a single hidden vector decay and have a relatively simple substructure, additional radiation or substructure tends to degrade the efficiency of these cuts [11,36]. It would also be interesting to study the prospects of identifying tauonic or hadronic HV jets that also arise frequently for these sample points based on their collimated substructure, but such an investigation is beyond the scope of the present work.

Benchmark points HV3 and HV5 contain displaced vector decays. These originate from $A^x \to h_1^x X^{\mu *}$ with the vector off shell for both points, and from $\chi_2^x \to \chi_1^x X^{\mu *}$ for HV5. Taking into account the net boost from the initial LSMP neutralino decay, these decays are displaced from the collision vertex by $\gamma c\tau \sim 10-50$ cm for HV3 and $\gamma c\tau \sim 10-50$, $0.1-1$ cm (A^x and χ_2^x) for HV5. Such decay lengths will lead to displaced vertices in the tracking systems of the ATLAS and CMS detectors [33]. Even so, the small number of associated tracks (typically two) and the low invariant masses of the vector decay products could make these displaced decays difficult to distinguish from photon conversions in the detectors [33, 37]. Longer decay lengths, emerging outside the ATLAS and CMS tracking chambers, would be much more difficult to identify.

5.3 Collider Signals

Our analysis thus far has been based on the particle decay tables for the hidden sector and LSMP. While a full simulation of experimental factors is beyond to scope of the current paper, we have initiated a parton-level analysis of events at the 7 TeV LHC. Since our focus is on the hidden valley phenomenology, we used a simple MSSM spectrum with a 300 GeV Bino-like neutralino, an 800 GeV gluino, and all other new states heavy ($\gtrsim 2.5$ TeV). This is consistent with current LHC bounds from conventional supersymmetry searches [38], but will be probed by upcoming searches in the near future. The dominant production channel for these parameters is $pp \to \tilde{g}\tilde{g}$,

with a leading-order production cross section of about 200 fb. All other supersymmetric production processes are negligible, and in particular the pair production of the Binos has a cross section of 0.005 fb. Once created, the gluinos will decay to $q\bar{q}\chi_1^0$, so in addition to the two LSMP decay products discussed above, there will typically be four hard QCD jets in the final state.

For each of our sample points, we generated 50 000 events using MadGraph 4.4.49 [29], and then used BRIDGE 2.23 [30] to decay the gluino, Bino, and hidden sector particles. We modified the BRIDGE decay tables by hand to correctly include the hadronic contributions to the width. To simulate detector acceptances and efficiencies, we imposed a variety of parton-level cuts. All objects with pseudo-rapidity $|\eta| > 2.5$ were ignored. We defined an HV jet as consisting of at least two hard subobjects each with $p_T > 10$ GeV collimated within a cone of size $\Delta R < 0.1$ with an isolation cut of $\sum p_T < 3$ GeV within $0.1 < \Delta R < 0.4$ relative to the net momentum of the two hardest subobjects in the central cone. However, we did not distinguish between leptonic and hadronic HV jets, nor did we account for the some of the hidden decay products being displaced. Thus, our estimates of HV jet acceptance are likely to be overly optimistic. We also defined a (parton-level) QCD jet as consisting of one or more objects within $\Delta R = 0.4$ that fail the HV jet criteria and have a total $p_T > 20$ GeV. Lastly, we define the missing transverse energy $\not{E}_T$ as the sum of the transverse momenta of all jets and HV jets.

In Fig. 10 we show the distributions of missing energy for gluino-initiated events in sample points HV2–HV5. This includes the contribution from metastable hidden states decaying outside the detector. As already noted, the presence of several hard jets from the gluino decays will make such events easy to trigger on even when the hidden sector is completely invisible. We see that as the expected number of HV jets increases from HV1 to HV5, the missing energy distribution peaks at lower values. However, even for the most active benchmark points, the majority of supersymmetric events still have a significant amount of missing energy implying that the standard search channels for supersymmetry at the LHC will be sensitive to these sample points as well.

We show the tagging efficiencies for HV jets for HV2–5 in Table 4 (recall that HV1 does not produce HV jets). Some HV jets will fail to tag due to overlapping with other HV jets or the hard jets from gluino decay. However, the difference in tagging efficiency for the different benchmarks is mostly due to differences in the LSMP decay chains. Note that the tagging efficiency is

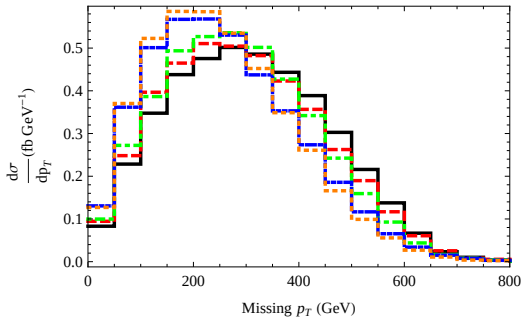

Figure 10: The $\not{E}_T$ distributions for the five benchmark points for gluino-initiated events. The solid black (red dashed, green dot-dashed, blue dot-dot-dashed, orange dotted) line corresponds to HV1 (HV2, HV3, HV4, HV5).

Benchmark	HV Jet Tag Efficiency
HV2	88%
HV3	50%
HV4	63%
HV5	54%

Table 4: Efficiencies to tag HV jets for the four benchmark points that produce them according to the requirements listed in the text.

much higher for HV2, where all HV jets come from the direct production of the hidden vector from the Bino. In contrast, the other three benchmarks involve longer decay chains through the hidden sector (HV4), three body decays out of the hidden sector (HV3) or both (HV5). Both effects lead to softer final state particles, and the products of three-body decays tend to be less collinear and have a broader spread in energy than when this decay is from an on-shell vector. This increases the fraction of candidate HV jets that are either too separated, $\Delta R > 0.1$, or fail to have two sufficiently hard ($p_T > 10$ GeV) seed partons.

We next show the distributions of the number of HV jets, and of distinct (parton-level) jets and HV jets combined in Fig. 11. Compared to the values of $P_0 \ldots P_4$ computed in Sec. 5.1, the HV jet number distribution here is smaller as expected from Table 4. However, by examining the distributions including (parton-level) jets we can see that a sizeable fraction of would-be

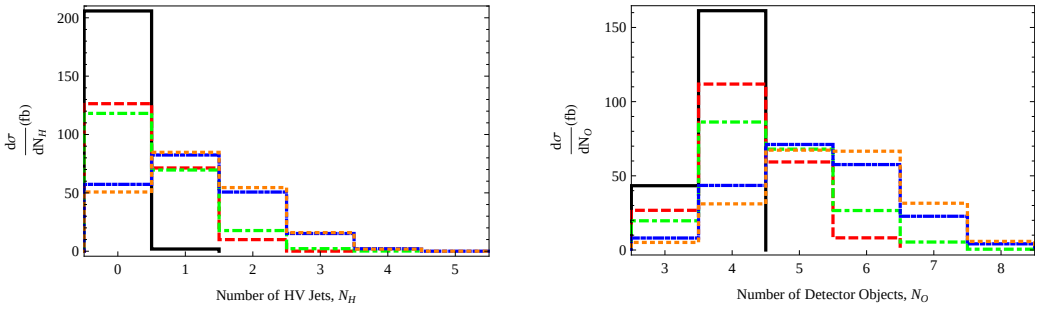

Figure 11: The distribution of the number of HV jets (left) and HV jets plus jets (right) in gluino-initiated events for our benchmark points. The solid black (red dashed, green dot-dashed, blue dot-dot-dashed, orange dotted) lines correspond to HV1 (HV2, HV3, HV4, HV5).

HV jets are still tagged as jets. This suggests that the tagging efficiency could be improved based on a closer study of the substructure of these objects.

In Fig. 12 we show the p_T distributions of the hardest HV jet in a given event for HV2–5. When we normalise the distribution to the total cross section for events with at least one HV jet, it is obvious that HV3 produces much softer HV jets than HV2, HV4 and HV5, with HV2 producing the hardest objects. This is caused by the same effects that lower the HV jet tagging efficiency, *i.e.* higher multiplicity of the final state. In Appendix C we show the p_T distributions for all HV jets produced in these benchmarks.

The last obvious characteristic of our sample points is the presence or absence of displaced vertices. We assign a cut on the distance to the appearance of the first visible object in a jet or HV jet of $d > 0.1$ mm to qualify as displaced. As expected from the discussion in Section 5.1, no events from HV2 or HV4 pass this requirement but a significant number from HV3 and HV5 do. We plot the total number of objects that qualify as displaced for HV3 and HV5 in Fig. 13. Note that displaced "ordinary jets" are visible decays in the hidden sector that fail the HV jet criteria but pass our jet conditions. Comparing these plots to Fig. 11, we see that in HV3 nearly all HV jets are displaced. In HV5, we see that when there is only a single HV jet, it is almost always displaced; only when there are multiple HV jets are any of them prompt. This is due to the Bino decay to $\chi_2^x X_\mu$ dominating over the $\chi_{1,3}^x X_\mu$ channels.

In Fig. 14. we plot the net displacements observed in simulated events

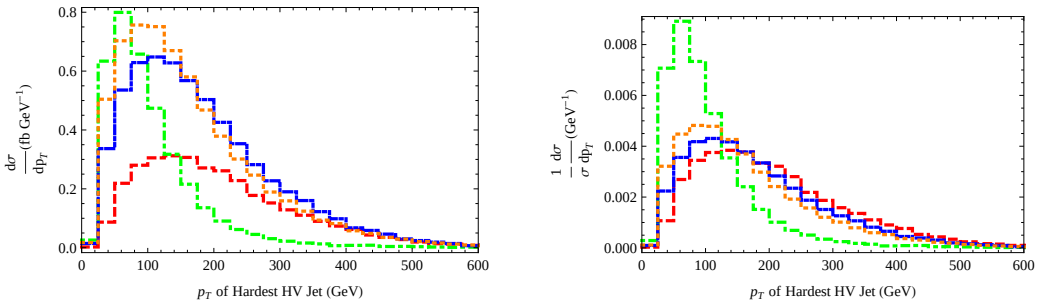

Figure 12: The p_T distributions for the hardest HV jets in gluino-initiated events. Left: the distributions for absolute cross-sections. Right: the distributions normalised to the total cross-section for events with at least one HV jet. The red dashed (green dot-dashed, blue dot-dot-dashed, orange dotted) lines correspond to HV2 (HV3, HV4, HV5).

for points HV3 and HV5. No collider resolution effects have been imposed beyond the lower displacement bound of 0.1 mm. The distribution for HV3 has a single peak near $d \simeq 40\,\text{cm}$ corresponding to the slow decays $A^x \to h_1^x {X_\mu}^*$. More interestingly, the distribution for HV5 has two distinct peaks in the distribution of decay lengths. These correspond to the two slow decay channels $A^x \to h_1^x {X_\mu}^*$ and $\chi_2^x \to \chi_1^x {X_\mu}^*$. Observing such a "double bump" feature could be helpful in distinguishing the hidden sector decay chains.

So far we have only investigated LHC collider events initiated by gluino pair production. Direct electroweak production of neutralinos (and charginos) could also lead to interesting signals if they produce visible HV jets. This possibility was investigated in Refs. [10–12], where it was assumed that the hidden sector produced two HV jets in every LSMP neutralino decay for a total of four in each supersymmetric event. In our specific and explicit realization of a supersymmetric hidden sector, we find that most supersymmetric events produce many fewer HV jets. A particularly distinctive possibility for direct neutralino production that arises in our scenario are events with HV monojets, consisting of a single visible HV jet accompanied by missing energy. Existing LHC monojet searches [39] do not bound our sample MSSM spectrum since the production cross section for a 300 GeV Bino-like neutralino is extremely small (0.005 fb), but such searches with existing and upcoming data could be relevant for smaller masses or Wino- or Higgsino-like neutralinos [10, 11].

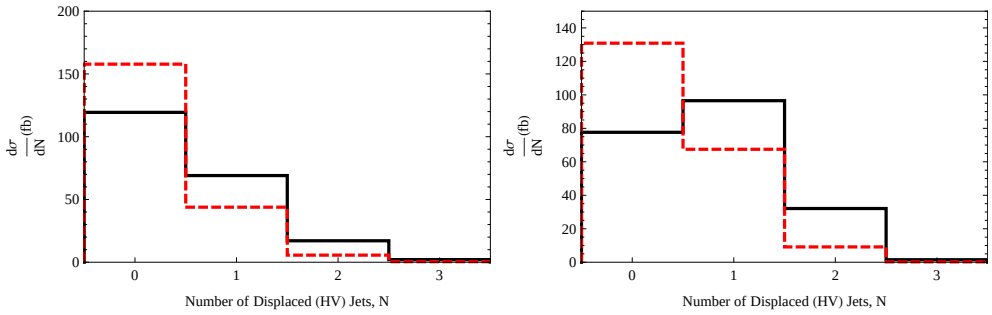

(a) HV3 (b) HV5

Figure 13: The number of displaced objects for the two benchmark points with off-shell hidden sector decays. Solid black (dashed red) lines represent HV jets (ordinary jets) with displacement greater than 1 mm from the primary vertex.

Benchmark	Monojet Branching Ratio
HV1	0%
HV2	26%
HV3	11%
HV4	18%
HV5	12%

Table 5: Branching ratios for pair production of 300 GeV LSMPs to monojets; see text for details.

To this end, we show in Table 5 the fraction of events for each benchmark where pair production of promptly-decaying neutralinos leads to a monojet event. We use the monojet definition of Ref. [39], specifically one jet (including HV jets) with $p_T > 120$ GeV, no other objects with $p_T > 30$ GeV, and missing energy $\not{E}_T > 120$ GeV. HV2 produces such events most frequently, due to producing hard HV jets and having a small P_2, see Fig. 12 and Table 2. HV4 and HV5 tend to produce high-multiplicity final states, while objects in HV3 are soft. Even so, all four points could be interesting in this channel for an appropriate LSMP. Distinguishing HV jets from ordinary QCD jets would further extend the reach of such searches.

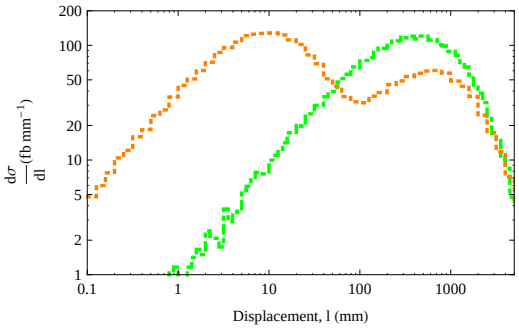

Figure 14: The distribution of hidden decay lengths from the primary vertex point for HV3 (green, dot-dashed) and HV5 (orange, dotted).

6 Conclusions

We have presented and investigated the collider signals of a simple and minimal example of a supersymmetric hidden valley. The theory consists of the MSSM together with a hidden sector consisting of a $U(1)_x$ vector multiplet and a pair of chiral Higgs multiplets. These two sectors interact with each other exclusively through supersymmetric gauge kinetic mixing. We assume that the hidden sector feels supersymmetry breaking less directly than the visible MSSM sector, and has a characteristic mass scale (and spontaneous breakdown of $U(1)_x$) near a GeV.

The light hidden sector can give rise to new and unusual signals at high energy particle colliders such as the LHC. MSSM superpartners will be created in the usual way and decay in a cascade down to the lightest MSSM superpartner (LSMP). In turn, the LSMP will decay into the hidden sector by way of the kinetic mixing interaction. The decay cascade will continue within the hidden sector, and one or more $U(1)_x$ vector bosons can be produced along the way. Depending on the hidden spectrum, the vector will frequently decay exclusively to pairs of light SM particles. Thus, the continuation of the supersymmetric cascade into the hidden sector can give rise to additional *visible* particles in the final state characteristic of a hidden valley.

In the present work we have studied the collider signals of the specific case of a neutralino LSMP. We find boosted HV jets of collimated leptons or hadrons, missing energy, and multiple displaced vertices for various parameter values in the hidden sector. More general sets of MSSM and hidden

sector parameters could also give rise to heavy-flavour jets, charged track stubs, long-lived coloured particles, and much else. The broad range of new and unusual collider signals that can arise in this simple theory makes it a useful benchmark model with which to investigate the sensitivity and feasibility of LHC searches for hidden valleys.

Acknowledgements

We thank Anadi Canepa, David Poland, Matthew Strassler, Oliver Stelzer-Chilton, Itay Yavin, and Kathryn Zurek for helpful discussions. We also thank an anonymous referee for critical comments that helped improve this work. DM would like to thank the Perimeter Institute for their hospitality during the completion of this work. This research is supported by NSERC.

A Appendix: Hidden Sector Interactions

We collect here the relevant interactions within the hidden sector, written in terms of the mass eigenstates. We work in the unitary gauge, and our definitions of the mass eigenstates and mixing angles follows the conventions specified in Section 2.2. We also keep terms only up to linear order in the small kinetic mixing ϵ.

A.1 Gauge Interactions

The relevant hidden sector fermion gauge couplings are

$$\begin{aligned} -\mathcal{L} &\supset -i\tilde{H}^\dagger \bar{\sigma}^\mu(\partial_\mu + ig_x X'_\mu)\tilde{H} - i\tilde{H}'^\dagger \bar{\sigma}^\mu(\partial_\mu - ig_x X'_\mu)\tilde{H}' \\ &\supset g_x(P_{i1}P^*_{j1} - P_{i2}P^*_{j2})\chi_i^{x\dagger}\bar{\sigma}^\mu(X'_\mu)\chi_j^x \,, \end{aligned} \tag{39}$$

where $X'_\mu = (X_\mu + \epsilon\, s_W Z_\mu)$.

For the scalars, we have

$$\begin{aligned} -\mathcal{L} &\supset -\left|(\partial_\mu + ig_x X'_\mu)H\right|^2 - \left|(\partial_\mu - ig_x X'_\mu)H'\right|^2 \\ &\supset g_x(c_\zeta R_{1a} - s_\zeta R_{2a})X'^\mu(A^x\cdot\partial_\mu h_a - \partial_\mu A^x\cdot h_a) \\ &\quad -\frac{1}{2}g_x^2(X'_\mu)^2(h_1^2 + h_2^2 + A^{x2}) - \sqrt{2}g_x^2(R_{1a}s_\zeta + R_{2a}c_\zeta)\eta(X'_\mu)^2 h_a \,. \end{aligned} \tag{40}$$

Note that we have dropped various kinetic and mass terms along the way.

A.2 Yukawa Interactions

The relevant terms involving only hidden sector fields are

$$\begin{aligned} -\mathcal{L} &\supset \sqrt{2}g_x H^* \tilde{H}\tilde{X} - \sqrt{2}g_x H'^* \tilde{H}'\tilde{X} + (h.c.) \\ &\supset g_x(R_{1a}P^*_{i1}P^*_{j3} - R_{2a}P^*_{i2}P^*_{j3})h_a \chi^x_i \chi^x_j \\ &\quad -ig_x(c_\zeta R^*_{i1}R^*_{j3} - s_\zeta P^*_{i2}P^*_{j3})A^x \chi^x_i \chi^x_j + (h.c.) \end{aligned} \tag{41}$$

These couplings are the supersymmetric partners of the vector boson couplings given above.

There are also interactions with the visible Bino due to the kinetic mixing shift of Eq. (12). This leads to

$$\begin{aligned} -\mathcal{L} &\supset -\epsilon\sqrt{2}g_x H^* \tilde{H}\tilde{B} + \epsilon\sqrt{2}g_x H'^* \tilde{H}'\tilde{B} + (h.c.) \\ &\supset -g_x(R_{1a}P^*_{i1}N^*_{j1} - R_{2a}P^*_{i2}N^*_{j1})h_a \chi^x_i \chi^0_j \\ &\quad +ig_x(c_\zeta P^*_{i1}N^*_{j1} - s_\zeta P^*_{i2}N^*_{j1})A^x \chi^x_i \chi^0_j + (h.c.) \end{aligned} \tag{42}$$

These couplings are crucial to allowing the MSSM LSP to decay to the lighter hidden sector states.

A.3 Scalar Interactions

These derive from the D-term:

$$\begin{aligned} -\mathcal{L} &\supset \frac{g_x^2}{2}\left(|H|^2 - |H'|^2\right)^2 \\ &\supset \frac{1}{2}g_x m_x \left(s_\zeta R_{1a} - c_\zeta R_{2a}\right)\left[(R_{1c}R_{1d} - R_2 c R_{2d})\right] h_c h_d + c_{2\zeta}A^{x2}\big] \; h_a + \ldots \end{aligned} \tag{43}$$

In the last line we have omitted various 4-point scalar couplings that are less important for the collider phenomenology.

A.4 Mass Mixing with the MSSM

Mass mixing between the visible and hidden sectors can largely be neglected to an excellent approximation. Such mixing is suppressed by powers of both ϵ and m_x/m_{MSSM}, leading to very small mixing angles. However, as discussed in the text, there are two situations where hidden-visible mass mixing can play an important role in the collider signatures of the theory, and we address the issue here.

Since the relevant mixing angles are very small, we can treat the mass mixing as a two-point interaction between purely hidden and visible mass eigenstates. The first situation of interest is the mass mixing between the Bino and the hidden Higgsinos arising from Eq. (18). This induces the fermion mass mixing interaction

$$-\mathcal{L} \supset -\epsilon\, m_x \left(s_\zeta P^*_{i1} N^*_{j1} - c_\zeta P^*_{i2} N^*_{j1}\right) \chi^x_i \chi^0_j \,. \tag{44}$$

By mixing into the hidden Higgsino, the LSMP neutralino develops a coupling to the hidden vector. In LSMP decays, the mass-ratio suppression in the mixing angle is cancelled by the enhanced coupling to the longitudinal component of the vector.

The second situation where hidden-visible mass mixing can play an important role in the phenomenology arises for the lightest CP-even hidden Higgs. Its mass-mixing interaction with the SM Higgs boson derives from the mixed D-term interaction and is given by

$$\begin{aligned} -\mathcal{L} \;&\supset\; -\epsilon\, D_x D_Y \\ &\supset\; \epsilon\, s_W\, m_x m_Z \left(s_\zeta R_{1a} + c_\zeta R_{2a}\right) \\ &\qquad \times \left[(s_\beta \tilde{c} - c_\beta \tilde{s})\, h^0 + (s_\beta \tilde{s} + c_\beta \tilde{c})\, H^0\right] h^x_a \,. \end{aligned} \tag{45}$$

Even though this coupling leads to a very small mass mixing, it can still play an important role in the decay of the lightest CP-even hidden Higgs as we discuss in Section 3.2.

B Appendix: Benchmark Point Parameters

We list here the underlying hidden sector parameter points for the five benchmark points discussed in Section 5. Recall that $g_x = 0.3$ and $\epsilon = 10^{-3}$ is assumed throughout.

	m_x (GeV)	m_{A^x} (GeV)	μ' (GeV)	M_x (GeV)	$\tan\zeta$
HV1	5.73	0.60	−7.47	1.69	6.48
HV2	0.65	7.43	−1.09	0.32	0.92
HV3	6.49	4.04	−2.52	1.21	1.85
HV4	0.90	9.72	−1.83	0.28	0.39
HV5	3.53	3.00	3.51	8.41	0.39

C Appendix: Additional Plots

We collect here some additional plots related to the discussion of Section 5.3. In Fig. 15 we show the p_T distributions for the four hardest HV jets for the sample points HV2–HV5. Recall that HV1 has no HV jets.

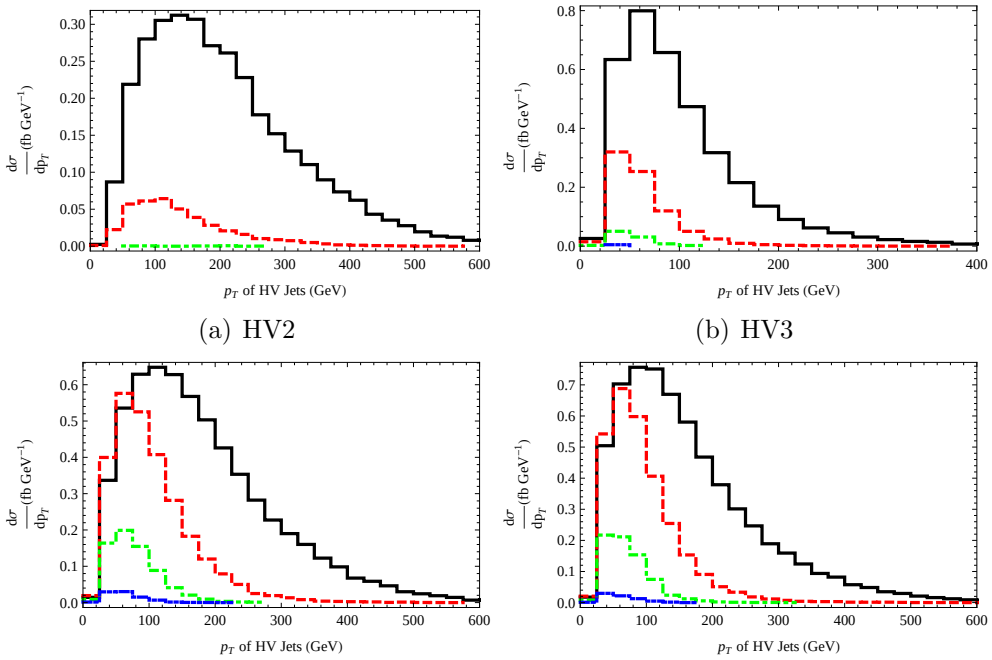

(a) HV2 (b) HV3

(c) HV4 (d) HV5

Figure 15: The p_T distributions of the HV jets for the four benchmark points 2–5. The first (second, third, fourth) hardest jets are denoted by solid black (dashed red, dot-dashed green, dot-dot-dashed blue) lines.

References

[1] D. Alves, N. Arkani-Hamed, S. Arora, Y. Bai, M. Baumgart, *et. al.*, *Simplified Models for LHC New Physics Searches*, arXiv:1105.2838. * Temporary entry *. D. E. Morrissey, T. Plehn, and T. M. Tait, *Physics searches at the LHC*, arXiv:0912.3259.

[2] M. J. Strassler and K. M. Zurek, *Echoes of a hidden valley at hadron colliders*, *Phys.Lett.* **B651** (2007) 374–379, [hep-ph/0604261].

[3] M. J. Strassler, *Possible effects of a hidden valley on supersymmetric phenomenology*, hep-ph/0607160.

[4] M. J. Strassler and K. M. Zurek, *Discovering the Higgs through highly-displaced vertices*, *Phys.Lett.* **B661** (2008) 263–267, [hep-ph/0605193]. T. Han, Z. Si, K. M. Zurek, and M. J. Strassler, *Phenomenology of hidden valleys at hadron colliders*, *JHEP* **0807** (2008) 008, [arXiv:0712.2041].

[5] N. Arkani-Hamed, D. P. Finkbeiner, T. R. Slatyer, and N. Weiner, *A Theory of Dark Matter*, *Phys.Rev.* **D79** (2009) 015014, [arXiv:0810.0713]. C. Cheung, J. T. Ruderman, L.-T. Wang, and I. Yavin, *Kinetic Mixing as the Origin of Light Dark Scales*, *Phys.Rev.* **D80** (2009) 035008, [arXiv:0902.3246]. A. Katz and R. Sundrum, *Breaking the Dark Force*, *JHEP* **0906** (2009) 003, [arXiv:0902.3271].

[6] N. Arkani-Hamed and N. Weiner, *LHC Signals for a SuperUnified Theory of Dark Matter*, *JHEP* **12** (2008) 104, [arXiv:0810.0714].

[7] D. E. Morrissey, D. Poland, and K. M. Zurek, *Abelian Hidden Sectors at a GeV*, *JHEP* **0907** (2009) 050, [arXiv:0904.2567].

[8] J. E. Juknevich, D. Melnikov, and M. J. Strassler, *A Pure-Glue Hidden Valley I. States and Decays*, *JHEP* **0907** (2009) 055, [arXiv:0903.0883]. K. L. McDonald and D. E. Morrissey, *Low-Energy Probes of a Warped Extra Dimension*, *JHEP* **1005** (2010) 056, [arXiv:1002.3361]. T. Gherghetta and B. von Harling, *A Warped Model of Dark Matter*, *JHEP* **1004** (2010) 039, [arXiv:1002.2967].

[9] B. Holdom, *Two U(1)'s and Epsilon Charge Shifts*, *Phys.Lett.* **B166** (1986) 196.

[10] M. Baumgart, C. Cheung, J. T. Ruderman, L.-T. Wang, and I. Yavin, *Non-Abelian Dark Sectors and Their Collider Signatures*, *JHEP* **0904** (2009) 014, [arXiv:0901.0283].

[11] C. Cheung, J. T. Ruderman, L.-T. Wang, and I. Yavin, *Lepton Jets in (Supersymmetric) Electroweak Processes*, *JHEP* **1004** (2010) 116, [arXiv:0909.0290].

[12] Y. Bai and Z. Han, *Measuring the Dark Force at the LHC*, *Phys.Rev.Lett.* **103** (2009) 051801, [arXiv:0902.0006].

[13] L. Carloni and T. Sjostrand, *Visible Effects of Invisible Hidden Valley Radiation*, *JHEP* **1009** (2010) 105, [arXiv:1006.2911].

[14] L. Carloni, J. Rathsman, and T. Sjostrand, *Discerning Secluded Sector gauge structures*, *JHEP* **1104** (2011) 091, [arXiv:1102.3795].

[15] G. Giudice and A. Masiero, *A Natural Solution to the mu Problem in Supergravity Theories*, *Phys.Lett.* **B206** (1988) 480–484.

[16] P. Fayet and J. Iliopoulos, *Spontaneously Broken Supergauge Symmetries and Goldstone Spinors*, *Phys.Lett.* **B51** (1974) 461–464.

[17] P. Z. Skands, B. Allanach, H. Baer, C. Balazs, G. Belanger, *et. al.*, *SUSY Les Houches accord: Interfacing SUSY spectrum calculators, decay packages, and event generators*, *JHEP* **0407** (2004) 036, [hep-ph/0311123].

[18] R. Essig, P. Schuster, and N. Toro, *Probing Dark Forces and Light Hidden Sectors at Low-Energy e+e- Colliders*, *Phys.Rev.* **D80** (2009) 015003, [arXiv:0903.3941].

[19] M. Reece and L.-T. Wang, *Searching for the light dark gauge boson in GeV-scale experiments*, *JHEP* **0907** (2009) 051, [arXiv:0904.1743].

[20] J. D. Bjorken, R. Essig, P. Schuster, and N. Toro, *New Fixed-Target Experiments to Search for Dark Gauge Forces*, *Phys.Rev.* **D80** (2009) 075018, [arXiv:0906.0580].

[21] B. Batell, M. Pospelov, and A. Ritz, *Probing a Secluded U(1) at B-factories*, *Phys.Rev.* **D79** (2009) 115008, [arXiv:0903.0363].

[22] T. Gherghetta, G. F. Giudice, and J. D. Wells, *Phenomenological consequences of supersymmetry with anomaly induced masses*, *Nucl.Phys.* **B559** (1999) 27–47, [hep-ph/9904378].

[23] H. Baer, K.-m. Cheung, and J. F. Gunion, *A Heavy gluino as the lightest supersymmetric particle*, *Phys.Rev.* **D59** (1999) 075002, [hep-ph/9806361]. J. L. Hewett, B. Lillie, M. Masip, and T. G. Rizzo, *Signatures of long-lived gluinos in split supersymmetry*, *JHEP* **0409** (2004) 070, [hep-ph/0408248]. M. Fairbairn, A. Kraan, D. Milstead, T. Sjostrand, P. Z. Skands, *et. al.*, *Stable massive particles at colliders*, *Phys.Rept.* **438** (2007) 1–63, [hep-ph/0611040].

[24] J. M. Cornwall, D. N. Levin, and G. Tiktopoulos, *Derivation of Gauge Invariance from High-Energy Unitarity Bounds on the s Matrix*, *Phys.Rev.* **D10** (1974) 1145. B. W. Lee, C. Quigg, and H. Thacker, *Weak Interactions at Very High-Energies: The Role of the Higgs Boson Mass*, *Phys.Rev.* **D16** (1977) 1519.

[25] **Particle Data Group** Collaboration, K. Nakamura *et. al.*, *Review of particle physics*, *J.Phys.G* **G37** (2010) 075021.

[26] J. F. Donoghue, J. Gasser, and H. Leutwyler, *THE DECAY OF A LIGHT HIGGS BOSON*, *Nucl.Phys.* **B343** (1990) 341–368.

[27] M. J. Strassler, *On the Phenomenology of Hidden Valleys with Heavy Flavor*, arXiv:0806.2385.

[28] N. D. Christensen and C. Duhr, *FeynRules - Feynman rules made easy*, *Comput. Phys. Commun.* **180** (2009) 1614–1641, [arXiv:0806.4194].

[29] J. Alwall *et. al.*, *MadGraph/MadEvent v4: The New Web Generation*, *JHEP* **09** (2007) 028, [arXiv:0706.2334].

[30] P. Meade and M. Reece, *BRIDGE: Branching ratio inquiry / decay generated events*, hep-ph/0703031.

[31] P. Fayet, *U-boson production in e+ e- annihilations, psi and Upsilon decays, and Light Dark Matter*, *Phys.Rev.* **D75** (2007) 115017, [hep-ph/0702176]. M. Pospelov, *Secluded U(1) below the weak scale*, *Phys.Rev.* **D80** (2009) 095002, [arXiv:0811.1030].

[32] P. Schuster, N. Toro, and I. Yavin, *Terrestrial and Solar Limits on Long-Lived Particles in a Dark Sector*, *Phys.Rev.* **D81** (2010) 016002, [arXiv:0910.1602]. **APEX** Collaboration, S. Abrahamyan *et. al.*, *Search for a New Gauge Boson in Electron-Nucleus Fixed-Target Scattering by the APEX Experiment*, *Phys.Rev.Lett.* **107** (2011) 191804, [arXiv:1108.2750]. B. Batell, M. Pospelov, and A. Ritz, *Exploring Portals to a Hidden Sector Through Fixed Targets*, *Phys.Rev.* **D80** (2009) 095024, [arXiv:0906.5614]. **A1** Collaboration, H. Merkel *et. al.*, *Search for Light Gauge Bosons of the Dark Sector at the Mainz Microtron*, *Phys.Rev.Lett.* **106** (2011) 251802, [arXiv:1101.4091]. S. Andreas and A. Ringwald, *Status of sub-GeV Hidden Particle Searches*, arXiv:1008.4519.

[33] **CMS** Collaboration, G. Bayatian *et. al.*, *CMS technical design report, volume II: Physics performance*, *J.Phys.G* **G34** (2007) 995–1579. **ATLAS** Collaboration, G. Aad *et. al.*, *Expected Performance of the ATLAS Experiment - Detector, Trigger and Physics*, arXiv:0901.0512.

[34] **D0** Collaboration, V. Abazov *et. al.*, *Search for dark photons from supersymmetric hidden valleys*, *Phys.Rev.Lett.* **103** (2009) 081802, [arXiv:0905.1478]. **D0** Collaboration, V. M. Abazov *et. al.*, *Search for events with leptonic jets and missing transverse energy in* $\mathbf{p\bar{p}}$ *collisions at* $\sqrt{\mathbf{s}} = \mathbf{1.96}$ *TeV*, *Phys.Rev.Lett.* **105** (2010) 211802, [arXiv:1008.3356].

[35] A. Falkowski, J. T. Ruderman, T. Volansky, and J. Zupan, *Discovering Higgs Decays to Lepton Jets at Hadron Colliders*, *Phys.Rev.Lett.* **105** (2010) 241801, [arXiv:1007.3496].

[36] A. Falkowski, J. T. Ruderman, T. Volansky, and J. Zupan, *Hidden Higgs Decaying to Lepton Jets*, *JHEP* **1005** (2010) 077, [arXiv:1002.2952].

[37] **ATLAS** Collaboration, G. Aad *et. al.*, *Search for displaced vertices arising from decays of new heavy particles in 7 TeV pp collisions at ATLAS*, arXiv:1109.2242. * Temporary entry *.

[38] **ATLAS** Collaboration, G. Aad *et. al.*, *Search for supersymmetry with jets and missing transverse momentum: Additional model*

interpretations, ATLAS-CONF-2011-155. **CMS** Collaboration, *Search for supersymmetry in all-hadronic events with missing energy*, PAS-SUS-11-004.

[39] **ATLAS** Collaboration, G. Aad *et. al.*, *Search for new phenomena with the monojet and missing transverse momentum signature using the ATLAS detector in sqrt(s) = 7 TeV proton-proton collisions*, *Phys. Lett. B* **705** (2011) 294–312, [arXiv:1106.5327]. * Temporary entry *.